

5-1997

Structural Design of a Crashworthy Energy Absorbing Passenger Seat For a Large Transport Aircraft Using Large Displacement, Nonlinear Material Finite Element Analysis

Javier Fuentes

Embry-Riddle Aeronautical University - Daytona Beach

Follow this and additional works at: <https://commons.erau.edu/db-theses>



Part of the [Aviation Commons](#)

Scholarly Commons Citation

Fuentes, Javier, "Structural Design of a Crashworthy Energy Absorbing Passenger Seat For a Large Transport Aircraft Using Large Displacement, Nonlinear Material Finite Element Analysis" (1997). *Theses - Daytona Beach*. 285.

<https://commons.erau.edu/db-theses/285>

This thesis is brought to you for free and open access by Embry-Riddle Aeronautical University – Daytona Beach at ERAU Scholarly Commons. It has been accepted for inclusion in the Theses - Daytona Beach collection by an authorized administrator of ERAU Scholarly Commons. For more information, please contact commons@erau.edu.

**STRUCTURAL DESIGN OF A CRASHWORTHY ENERGY ABSORBING
PASSENGER SEAT FOR A LARGE TRANSPORT AIRCRAFT
USING LARGE DISPLACEMENT, NONLINEAR MATERIAL
FINITE ELEMENT ANALYSIS**

by

Javier A. Fuentes

A Thesis Presented to the

School of Graduate Studies and Research

In Partial Fulfillment of the Requirements for the Degree of

Master of Science in Aerospace Engineering

Embry-Riddle Aeronautical University

Daytona Beach, Florida

May 1997

UMI Number: EP31831

INFORMATION TO USERS

The quality of this reproduction is dependent upon the quality of the copy submitted. Broken or indistinct print, colored or poor quality illustrations and photographs, print bleed-through, substandard margins, and improper alignment can adversely affect reproduction.

In the unlikely event that the author did not send a complete manuscript and there are missing pages, these will be noted. Also, if unauthorized copyright material had to be removed, a note will indicate the deletion.

UMI[®]

UMI Microform EP31831
Copyright 2011 by ProQuest LLC
All rights reserved. This microform edition is protected against
unauthorized copying under Title 17, United States Code.

ProQuest LLC
789 East Eisenhower Parkway
P.O. Box 1346
Ann Arbor, MI 48106-1346

**STRUCTURAL DESIGN OF A CRASHWORTHY ENERGY ABSORBING
PASSENGER SEAT FOR A LARGE TRANSPORT AIRCRAFT
USING LARGE DISPLACEMENT, NONLINEAR MATERIAL
FINITE ELEMENT ANALYSIS**

by

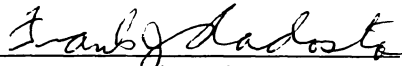
Javier A. Fuentes

This thesis was prepared under the direction of the candidate's thesis committee chairman, Dr. David Kim, Department of Aerospace Engineering, and has been approved by the members of this thesis committee. It was submitted to the Office of Graduate Studies and was accepted in partial fulfillment of the requirements for the degree of Master of Science in Aerospace Engineering.

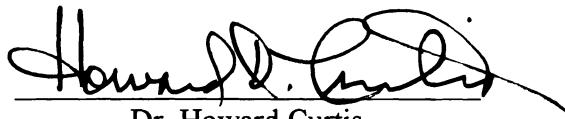
THESIS COMMITTEE



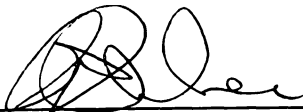
Dr. David Kim
Chairman



Dr. Frank Radosta
Member



Dr. Howard Curtis
Member



Department Chair, Aerospace Engineering



Date

ACKNOWLEDGMENTS

I would like to thank God for everything. Thanks to my parents for providing moral and financial support every step of the way. Thanks to my sister for being there. Thanks to my aunt for her help and support. Special thanks to Dr. David Kim and Dr. Frank Radosta for the valuable help and time throughout my research. Thanks to Dr. Howard Curtis for being part of my thesis committee. Thanks to Charles Bishop for providing a teaching assistantship. Thanks to Darryl Marsee and Eric Sorton for their help in running ABAQUS. I would also like to thank Perki, Ron and Duane for being there the last three years. Thanks to How Meng Au for his help in drawing figures. Thanks to Marcela for her support during the last few months. Thanks to all those who are not mentioned here that in one way or another help me through my graduate studies.

ABSTRACT

Author: Javier Fuentes

Title: Structural Design of a Crashworthy Energy Absorbing Passenger Seat For a Large Transport Aircraft Using Large Displacement, Nonlinear Material Finite Element Analysis

Institution: Embry-Riddle Aeronautical University

Degree: Master of Science in Aerospace Engineering

Year: 1997

Federal Aviation Regulations certification criteria for transport aircraft seats require performing dynamic tests using anthropomorphic test dummies. Floor decelerations of the tests are 16g forward with the seat tracks misaligned by up to 10 degrees and 14g downward at a pitch angle of 30 degrees. In this project the dynamic response of the passenger/seat/restraint system is modeled using nonlinear finite element analysis. The interference between a dummy model and the seat is modeled using a contact interaction algorithm. This algorithm did not converge and multiple-point constraints were used to transfer the dummy's inertia load. This approach was validated with the software SOM-TA and then used to predict the response of a high energy absorption seat design subjected to the floor deceleration as stated in the FAR. The seat withstood the dynamic loading in both cases. The seat showed poor energy absorption characteristics when subjected to the 14g downward floor deceleration.

TABLE OF CONTENTS

	Page
Acknowledgments.....	iii
Abstract.....	iv
List of Tables.....	vii
List of Figures.....	viii
1. INTRODUCTION.....	1
1.1. Overview.....	1
1.2. Background.....	4
1.3. FAR Requirements.....	6
2. FINITE ELEMENT METHOD.....	8
2.1. Static Analysis.....	8
2.1.1. Displacement-Based Finite Element Formulation.....	13
2.2. Nonlinear Analysis.....	18
2.2.1. Newton-Raphson Method.....	19
2.2.2. Modified Newton-Raphson Method.....	20
2.2.3. Contact Problem Overview.....	23
2.3. Dynamic Analysis.....	27
2.3.1. Damping.....	31
2.3.2. Direct Integration Methods.....	32
2.3.2.1. Central Difference Method.....	33
2.3.2.2. Newmark Method.....	35
2.4. ABAQUS.....	36
3. VALIDATION OF PASSENGER-SEAT INTERFERENCE.....	38
3.1. General.....	38
3.2. Dummy Model Description.....	38
3.2.1. Model Segment Definition.....	39
3.2.2. Model Joint Characteristics.....	42
3.3. Seat Model Description.....	45
3.4. Dummy-Seat Interaction.....	47
3.5. Analysis of Results.....	51
4. ENERGY-ABSORPTION SEAT DESIGN.....	59
4.1. Design Consideration.....	59
4.2. Energy-Absorbing Seat Description.....	60

4.3. Dynamic Test Simulation Results of the Energy-Absorbing Seat.....	66
5. CONCLUSIONS AND RECOMMENDATIONS.....	76
5.1. Conclusions.....	76
5.2. Recommendations.....	78
REFERENCES.....	79

LIST OF TABLES

	Page
Table 1. Degrees of Freedom in Joints of the Dummy Model.....	45
Table 2. Seat Model Displacement Comparison in the X,Y and Z axis at t=0.025 s.....	55
Table 3. Seat Model Displacement Comparison in the X,Y and Z axis at t=0.175 s.....	55

LIST OF FIGURES

	Page
Figure 1. Newton-Raphson Incremental Solution.....	21
Figure 2. Modified Newton-Raphson Incremental Solution.....	22
Figure 3. Two Meshes of a FE Model that (a) May come into contact, (b) Slide with respect to each other.....	23
Figure 4. Stress-Strain Relationship for a gap element in the (a) Normal Direction, (b) Tangential Direction.....	25
Figure 5. Pressure-Clearance Relationship for (a) 'hard' contact (b) 'softened' contact.....	27
Figure 6. Three-Dimensional Representation of the Dummy Model.....	40
Figure 7. Rigid Elements Local Coordinate System.....	41
Figure 8. Illustration of Typical Joint Test Curve.....	43
Figure 9. Joint Torque Approximation Curve.....	43
Figure 10. Three-Dimensional Sketch of the Seat Used for the Validation.....	46
Figure 11. Passenger/Seat Model Representation.....	50
Figure 12. Lap Belt Force Comparison Between ABAQUS and SOM-TA Model Response.....	52
Figure 13. Time-History Response of the Dummy with respect to the X axis compared to SOM-TA's.....	54
Figure 14. Time-History Response of the Dummy with respect to the Z axis compared to SOM-TA's.....	54
Figure 15. Illustration of Particular Nodes in the Seat Structure.....	57
Figure 16. Von-Mises Failure Criteria at $t=0.223$ s.....	58
Figure 17. Dimensional Layout of Energy-Absorbing Seat.....	61

Figure 18. Structural Components of the Energy-Absorbing Seat.....	62
Figure 19. Cross-Sections of Structural Members of the Seat.....	63
Figure 20. Inversion tube Load-Deflection Characteristics.....	65
Figure 21. Von-Mises Failure Criteria after Seat Track Deformation.....	67
Figure 22. Forward Seat Deformation at $t=0.17$ s.....	68
Figure 23. Lateral Deformation Contour of the seat.....	69
Figure 24. Time-History Compressive Stress of the Left Energy Absorber.....	70
Figure 25. Force-Deflection Curve of the Left Energy-Absorber for 16g Forward test.....	71
Figure 26. Three-Dimensional Illustration of the Deformed Seat.....	72
Figure 27. Forward Deformation on the seat due to 14g floor deceleration.....	74
Figure 28. Von-Mises Failure Criteria for 14g Downward Deceleration.....	75

1. INTRODUCTION

1.1. Overview

Analyses of transport aircraft accidents that occurred between 1970 and 1985 showed that failure of seats and other cabin furnishings occurred frequently in survivable accidents¹. A survivable accident is “an accident in which the forces transmitted to the occupant through his seat and restraint system do not exceed the limits of human tolerance to abrupt accelerations and in which the structure in the occupant’s immediate environment remains substantially intact to the extent that a livable volume is provided for the occupant throughout the crash event.”² The failure of the seat/restraint system was determined as the cause of a great number of fatalities. Most of the failures occurred in the seat legs and their attachment points at the tracks. This proved that seat/restraint systems did not provide adequate protection to the passenger in survivable accidents and minimum design criteria established by the Federal Aviation Regulations did not adequately reflect survivable crash events². At the time, the structural loads the seat had to withstand for certification were 9g forward, 3g sideward, 2g upward and 6g downward. These static requirements were revised in 1988 and dynamic test standards were introduced as part of the certification requirement in part 25.562 of the Federal Aviation Regulations. Dynamic tests require the demonstration of both occupant response and seat/restraint system structural performance³. One test condition consists of a forward seat test with 10 degrees of yaw and a minimum deceleration of 16g. The seat tracks must be misaligned in the roll and pitch axes prior to testing to simulate floor

warping effects. The second test is performed with a forward pitch angle of 30 degrees and a minimum deceleration of 14g. These tests try to simulate the seats ability to withstand dynamic loading under typical crash scenario while preventing or minimizing serious injuries to the occupant. Head acceleration, pelvis and vertebral column loads are parameters used to evaluate passenger injuries.

The seat/restraint system serves as the link between the passenger and the aircraft floor. Its function is to support and restrain the passengers. During a crash, the seat/restraint system is the structural component that has one of the most direct effects on the passenger's survivability⁴ It represents the interface between the passenger and the airframe through which the crash inertia loads are transmitted. In survivable crash environments, the seat/restraint system must keep the passenger restrained, reduce injuries and provide sufficient opportunity to egress after the crash⁴ To accomplish this, the seat must carry the inertia loads of the passenger while remaining attached to the floor tracks, reduce the hazards of impact with other cabin furnishing (especially the seat in front) and leave enough volume to allow a successful evacuation.

When 'semi-rigid', nonyielding seats are subjected to the dynamic tests described above the loads induced in the seat structure and tracks exceed their failure limit loads⁵ Seats must be designed to absorb some of the crash energy. Energy-absorbing mechanisms can efficiently limit loads within the seat structure to levels below failure.

Energy-absorbing seats use structural members that can undergo large plastic deformations before failure. These members are called energy-absorbers and are usually

placed in the seat legs. Energy absorbing seats help reduce accelerations transmitted to the passenger, which translates directly into greater chance of survivability.

Current regulations require seats to undergo dynamic tests to achieve certification. Seats need to be manufactured without knowing a priori whether they will pass these tests and how well they will perform under dynamic conditions. Although analytical methods are contemplated in the regulation, they can only be considered as a means of certification when they can accurately predict failure mechanisms of the seat/restraint system and performance of the passenger for a variety of seat designs²

This study uses analytical tools to predict seat/restraint system performance when subjected to dynamic loading, as established in the emergency landing conditions section of the Federal Aviation Regulations. A Finite Element Analysis program (ABAQUS) is used to model this problem. The response of the passenger and seat/restraint system requires that both material and geometric nonlinear effects are included in the solution. Output from a computer program developed by the FAA is used to compare and validate the seat dynamic response predicted by a model built in ABAQUS.

The objective of this thesis is to design an energy-absorbing seat that can withstand the dynamic tests prescribed by the regulations and in the process assess ABAQUS capabilities as a finite element analytical tool to model nonlinear dynamic problems of this nature as compared to the program developed by the FAA.

Energy-absorbing seats have been developed by commercial seat manufacturers. Information on these seats is not available due to the fact that it is proprietary and confidential. Although there have been previous energy absorption seat designs the

purpose of this thesis is to develop a particular design that can successfully protect the passenger in the event of a survivable crash.

1.2. Background

Several mathematical models have been developed to analyze the response of human bodies to severe acceleration loads experienced during vehicle crashes. The complexity of these models range from a one degree of freedom system to predict injury in the vertebral column to three dimensional 40 degree of freedom models of a passenger. Most of the research in this area has been conducted by the automotive industry. Complex mathematical models of passengers have been developed to analyze their response to impact conditions. They are used as design tools to evaluate automobile interior designs and to predict the effects of restraint systems on their occupants. These models do not analyze the response of the seat because, in an automobile crash, the design of the seat has minimal effect on the occupant survivability.

SOM-TA (Seat/Occupant Model-Transport Aircraft) is a computer program created to aid the design and analysis of crashworthy transport aircraft seats and restraint systems. It was developed in 1986 by Simula, Inc., under a multi-million dollar contract with the FAA. It simulates the performance of three-dimensional passenger/seat models under crash conditions. Several computer programs were developed prior to this one to analyze occupant responses but are much more simplistic than SOM-TA. For this reason the discussion is limited to SOM-TA.

SOM-TA is based on a similar program developed by Simula for use with general aviation aircraft seats, called SOM-LA (Seat/Occupant Model Light Aircraft). This program was modified to model up to three passengers and define more complex transport aircraft seat structures. The purpose of this program was to provide seat manufacturers with an analytical tool to predict passenger and seat/restraint systems response under any given set of aircraft impact conditions.

The program uses finite element methods to model the aircraft seat structure and passenger responses. SOM-TA has the capability to model large displacements, nonlinear material behavior and local buckling⁶. Three dimensional beam elements are the only elements available to define the seat structure. SOM-TA was designed to minimize the volume of input data, particularly, passenger model characteristics. It has a built-in database of passenger models.

The passenger can be modeled in two or three dimensions. The three-dimensional mathematical model is made up of twelve rigid elements. For cases where symmetrical response is expected the option of a two-dimensional model is provided to achieve an economical program solution⁶. This model consists of 9 rigid elements and two beam elements to model the vertebral column and neck. These beam elements provide a measure of vertebral and neck loading to compare against an injury criteria. Interface between the seat and the occupant is provided through seat cushions and the restraint system. External forces are applied to the occupant by the seat cushions, floor and restraint systems. SOM-TA has the capability of modeling contact forces between the passenger and the seat cushion and floor.

SOM-TA provides time-history output of passenger 'segment' displacements, restraint system loads and contact forces at cushions. It also provides output of stresses in all the structural elements and loads at attachment points.

Dynamic tests of transport aircraft seats conducted in the former Civil Aeromedical Institute in 1983 helped the validation of the program⁷ The test of a production seat modified by incorporating energy-absorbers was used to validate SOM-TA.

1.3. FAR Requirements

In order for a transport aircraft seat to be certified as flightworthy, it must fulfill the FAR requirement set forth in 14 CFR 25.562(b) - Emergency Landing Dynamic Conditions:

“Each seat type design approved for crew or passenger occupancy during takeoff and landing must successfully complete dynamic tests or be demonstrated by rational analysis based on dynamic tests of a similar type seat, in accordance with each of the following emergency landing conditions. The test must be conducted with an occupant simulated by a 170-pound anthropomorphic test dummy, as defined by 49 CFR part 572, subpart B, or its equivalent, sitting in the normal upright position.

(1) A change in downward vertical velocity of not less than 35 feet per second, with the airplane's longitudinal axis canted downward 30 degrees with respect to the horizontal plane and with the wings level. Peak floor deceleration must occur in not more than 0.08 seconds after impact and must reach a minimum of 14g.

(2) A change in forward longitudinal velocity of not less than 44 feet per second, with the airplane's longitudinal axis horizontal and yawed 10 degrees either right or left, whichever would cause the greatest likelihood of the upper torso restraint system (where installed) moving off the occupant's shoulder, and with the wings level. Peak floor deceleration must occur in not more than 0.09 seconds after impact and must reach a minimum of 16g. Where floor rails or floor fittings are used to attach the seating devices to the test fixture, the rails or fittings must be misaligned

with respect to the adjacent set of rails or fittings by at least 10 degrees vertically (i.e., out of parallel) with one rolled 10 degrees”

2. FINITE ELEMENT METHOD

2.1. Static Analysis

Structural finite element analysis is a numerical technique used to solve complex structural problems that would otherwise be unsolvable using classical, closed-form, analytical methods. The behavior of a structure or continua is described by the stress-strain, equilibrium and compatibility (partial differential) equations⁸. The finite element method provides an approximate solution to these equations by discretizing or dividing the structure into subregions, i.e., elements, and expressing each element's state variables (displacement or stress) in terms of assumed shape functions. These functions are usually chosen so that the state variables or their derivatives are continuous and single valued across adjoining element boundaries⁹. Generally, polynomials have proven to provide the best and easiest representation. The shape functions, also called interpolating functions, provide approximate solutions and are defined in terms of the values of the state variables at specific points called nodes. Degrees of freedom (dof) are the nodal variables (unknowns) or parameters assigned to an element. Nodes are usually defined at the boundaries of the element and describe the shape of the element. Adjacent elements share common nodes. The finite element method solves for the values of the state variables at the nodes for a given set of initial conditions and loading. Using these values and the interpolation functions the state variable can be defined throughout the whole structure.

Most commercial Finite Element programs are displacement based, i.e., they express each element's behavior in terms of a piecewise continuous displacement field.

Each displacement field is defined in terms of the nodal dof associated with that element. The dof associated with each element are translation and rotation with respect to the X, Y and Z coordinate system. Using the Principle of Minimum Potential Energy, they provide the solution to the equations at the nodal dof. The stresses and strains in each element are computed from the displacements of the nodes, which are interpolated over the element. The degree of approximation of the solution depends on the number of dof of the model, which is set by the number of nodes and elements used. The higher the number of dof, the higher the degree of approximation at the expense of increased computer time and storage requirements. Excessive dof may introduce round-off errors due to the extreme number of calculations required for the solution.

The generalized Hooke's Law states that the stress at a point is expressed as a linear function of the strain within the linear range, as follows:

$$\{\sigma\} = [E]\{\varepsilon\} \quad [1]$$

where $\{\sigma\}$ is the stress vector, $\{\varepsilon\}$ is the strain vector and $[E]$ is a 6x6 matrix that represents the material dependent elastic constants. For an homogeneous and isotropic material, $[E]$ can be expressed in terms of two variables⁹, Young's Modulus E and Poisson's ratio ν . For a three dimensional state of stress, the isotropic stress-strain relationship can be expressed as:

$$\begin{bmatrix} \sigma_x \\ \sigma_y \\ \sigma_z \\ \tau_{xy} \\ \tau_{yz} \\ \tau_{xz} \end{bmatrix} = \begin{bmatrix} (1-\nu)c & \nu c & \nu c & 0 & 0 & 0 \\ \nu c & (1-\nu)c & \nu c & 0 & 0 & 0 \\ \nu c & \nu c & (1-\nu)c & 0 & 0 & 0 \\ 0 & 0 & 0 & G & 0 & 0 \\ 0 & 0 & 0 & 0 & G & 0 \\ 0 & 0 & 0 & 0 & 0 & G \end{bmatrix} \begin{bmatrix} \varepsilon_x \\ \varepsilon_y \\ \varepsilon_z \\ \gamma_{xy} \\ \gamma_{yz} \\ \gamma_{xz} \end{bmatrix} \quad [2]$$

where ν = Poisson's ratio and

$$c = \frac{E}{(1+\nu)(1-2\nu)}$$

$$G = \frac{E}{2(1+\nu)}$$

The equilibrium equations of a continuum are three partial differential equations.

Every infinitesimal element in a structure must satisfy these equations. For a three dimensional state of stress, the equations are:

$$\begin{aligned} \frac{\partial \sigma_x}{\partial x} + \frac{\partial \tau_{xy}}{\partial y} + \frac{\partial \tau_{xz}}{\partial z} + b_x &= 0 \\ \frac{\partial \sigma_y}{\partial y} + \frac{\partial \tau_{xy}}{\partial x} + \frac{\partial \tau_{yz}}{\partial z} + b_y &= 0 \\ \frac{\partial \sigma_z}{\partial z} + \frac{\partial \tau_{xz}}{\partial x} + \frac{\partial \tau_{yz}}{\partial y} + b_z &= 0 \end{aligned} \quad [3]$$

where the b 's are the body force densities.

The compatibility equations assert that the displacement field is continuous and single valued⁹ These equations are relations among the strains if the displacement field is compatible. Physically, the compatibility equations enforce the continuity of the structure; no voids, cracks, or overlaps are created in the deformed body if these were not existent prior to deformation⁸ The compatibility equations, written in terms of the state of strain, are:

$$\begin{aligned}
 \varepsilon_{xx,yy} + \varepsilon_{yz,xx} - \varepsilon_{xz,xy} - \varepsilon_{xy,xz} &= 0 \\
 \varepsilon_{yy,xz} + \varepsilon_{xz,yy} - \varepsilon_{xy,yz} - \varepsilon_{yz,xy} &= 0 \\
 \varepsilon_{zz,xy} + \varepsilon_{xy,zz} - \varepsilon_{yz,xz} - \varepsilon_{xz,yz} &= 0 \\
 2\varepsilon_{xy,xy} - \varepsilon_{xx,yy} - \varepsilon_{yy,xx} &= 0 \\
 2\varepsilon_{yz,yz} - \varepsilon_{yy,zz} - \varepsilon_{zz,yy} &= 0 \\
 2\varepsilon_{xz,xz} - \varepsilon_{zz,xx} - \varepsilon_{xx,zz} &= 0
 \end{aligned}
 \tag{4}$$

The compatibility condition is automatically satisfied by the displacement based finite element method.

The static problem of elastic solids is governed by 15 equations: 3 equilibrium, 6 strain-displacements and 6 stress-strain equations. The finite element method provides a piecewise continuous solution to the partial differential equations. The solution is continuous only within each elements boundaries partially satisfying the equilibrium equations¹⁰ The equilibrium equations are only satisfied at the nodes. The method solves for the values of the dof at the nodes. As the number of nodes increase the solution becomes more exact. In theory, if the number of nodes approaches infinity the equilibrium equations are completely satisfied and the solution becomes exact.

Realistically, however, too many nodes may reduce the accuracy due to the accumulated round-off errors.

For an elastic structure subjected to static loading, the applied forces are related to the resulting displacement field by

$$[K]\{D\} = \{R\} \quad [5]$$

where $[K]$ is the global stiffness matrix, $\{D\}$ is the column displacement vector, and $\{R\}$ is the applied loads column vector. The stiffness matrix is an $N \times N$ symmetric matrix, where N is the number of dof. If A is the number of nodes and B is the number of dof per node, $N = A \times B$. Vectors $\{D\}$ and $\{R\}$ have N columns. Each row in $\{D\}$ and $\{R\}$ corresponds to a possible displacement or force in the particular dof. Each dof has an associated term in the stiffness matrix.

The global stiffness matrix $[K]$ is the summation of the local stiffness matrices $[k]$ of all the elements that form the structure, i.e., $[K] = \sum [k]$. Each element contributes to the stiffness of the structure in one or several specific dof. Each term K_{ij} of the global stiffness matrix $[K]$ relates dof i in the global displacement column vector to dof j in the global load vector. A load applied to the i th dof will affect the deformation at the j th dof and viceversa.

To solve equation [5], applied forces and some displacements must be known. The known displacements are those of the supports of the structure (constrained dof), required to prevent rigid body motion. Equation [5] can be rearranged as:

$$\begin{bmatrix} K_{11} & K_{12} \\ K_{21} & K_{22} \end{bmatrix} \begin{Bmatrix} D_x \\ D_c \end{Bmatrix} = \begin{Bmatrix} R_x \\ R_c \end{Bmatrix} \quad [6]$$

where $\{D_x\}$ is the column vector of unknown displacements, $\{D_c\}$ is the column vector of known displacements, $\{R_x\}$ is the column vector of applied loads and $\{R_c\}$ is the column vector of unknown loads. Equation [6] can be rearranged as:

$$[K_{11}]\{D_x\} + [K_{12}]\{D_c\} = \{R_x\} \quad [7a]$$

$$[K_{21}]\{D_x\} + [K_{22}]\{D_c\} = \{R_c\} \quad [7b]$$

Solving for $\{D_x\}$ in equation [7a] yields

$$\{D_x\} = [K_{11}]^{-1}(\{R_x\} - [K_{12}]\{D_c\}) \quad [8]$$

Unknown loads can be found from equation [7b] after substitution of $\{D_x\}$. The strain of each element can be found using the element strain-displacement relationship. Using these strains and the stress-strain relationship the stresses at the nodes are determined.

2.1.1. Displacement-Based Finite Element Formulation

The Rayleigh-Ritz method in its classical form defines an approximate displacement field over the entire region of interest. An elastic solid has infinite dof.

These dof are the displacements of every material point¹⁰ The behavior of an elastic solid or continuum is described by partial differential equations. For complex and sometimes even simple structures, it is almost impossible to find the displacement field analytically that completely satisfies the partial differential equations⁹ The Rayleigh-Ritz method, as applied to finite element methods, discretizes the region of interest (structure) and defines a piecewise approximate displacement field for each element. This results in a problem that has a finite number of dof. The solution is not exact but the accuracy increases as the number of elements and hence the number of dof is increased. The Rayleigh-Ritz method uses the principle of stationary potential energy to formulate the problem, resulting in algebraic equations rather than differential equations¹⁰

Displacement-based elements are derived based on an approximate displacement field that are admissible. Admissible functions must satisfy compatibility conditions and essential boundary conditions (prescribed values for nodal dof)¹⁰ These conditions are best satisfied using polynomial functions.

The potential energy for a linearly elastic structure is the sum of the strain energy and the work performed by the external loads on the structure,

$$\begin{aligned} \Pi_p = & \int_V \left(\frac{1}{2} \{\boldsymbol{\varepsilon}\}^T [E] \{\boldsymbol{\varepsilon}\} - \{\boldsymbol{\varepsilon}\}^T [E] \{\boldsymbol{\varepsilon}_0\} + \{\boldsymbol{\varepsilon}\}^T \{\boldsymbol{\sigma}_0\} \right) dV \\ & - \int_V \{\mathbf{u}\}^T \{\mathbf{F}\} dV - \int_S \{\mathbf{u}\}^T \{\boldsymbol{\Phi}\} dS - \{\mathbf{D}\}^T \{\mathbf{P}\} \end{aligned} \quad [9]$$

where,

$\{u\} = [u \ v \ w]^T$, the displacement field in the respective X, Y and Z directions

$\{\epsilon\} = [\epsilon_x \ \epsilon_y \ \epsilon_z \ \gamma_{xy} \ \gamma_{yz} \ \gamma_{zx}]^T$, the strain field

$[E]$ = the material property matrix

$\{\epsilon_0\}, \{\sigma_0\}$ = initial strains and initial stresses

$\{F\} = [F_x \ F_y \ F_z]^T$, body forces

$\{\Phi\} = [\Phi_x \ \Phi_y \ \Phi_z]^T$, surface tractions

$\{D\}$ = nodal dof of the structure

$\{P\}$ = loads applied to dof by external agencies

S, V surface area and volume of the structure

Displacements within an element can be interpolated from elemental nodal dof $\{d\}$,

$$\{u\} = [N]\{d\} \quad [10]$$

where $[N]$ is the shape function matrix. Terms in $[N]$ are the interpolation functions that define how displacements vary throughout the element.

Strains are obtained by multiplying the differential operator matrix $[\partial]$ and the displacement vector $\{u\}$,

$$\begin{bmatrix} \varepsilon_x \\ \varepsilon_y \\ \varepsilon_z \\ \gamma_{xy} \\ \gamma_{yz} \\ \gamma_{xz} \end{bmatrix} = \begin{bmatrix} \frac{\partial}{\partial x} & 0 & 0 \\ 0 & \frac{\partial}{\partial y} & 0 \\ 0 & 0 & \frac{\partial}{\partial z} \\ \frac{\partial}{\partial y} & \frac{\partial}{\partial x} & 0 \\ 0 & \frac{\partial}{\partial y} & \frac{\partial}{\partial z} \\ \frac{\partial}{\partial x} & 0 & \frac{\partial}{\partial z} \end{bmatrix} \begin{bmatrix} u \\ v \\ w \end{bmatrix} \quad [11]$$

which, with equation [10], yields ,

$$\{\varepsilon\} = [B]\{d\}$$

where $[B] = [\partial][N]$ is the strain-displacement matrix.

Substituting expressions [10] and [11] into [9] yields,

$$\Pi_p = \frac{1}{2} \sum_{n=1}^{numel} \{d\}_n^T [k]_n \{d\}_n - \sum_{n=1}^{numel} \{d\}_n^T \{r_e\}_n - \{D\}^T \{P\} \quad [12]$$

where summations indicate that the contributions of all elements of the structure are included. The element stiffness matrix and the element load vector are defined as

$$[k] = \int_{V_e} [B]^T [E] [B] dV \quad [13]$$

$$\{r_e\} = \int_{V_e} [B]^T [E] \{\epsilon_o\} dV - \int_{V_e} [B]^T \{\sigma_o\} dV + \int_{V_e} [N]^T \{F\} dV + \int_{S_e} [N]^T \{\Phi\} dS \quad [14]$$

where V_e and S_e denote the volume and surface of an element, respectively. Every dof in an element vector $\{d\}$ also appears in the vector of global dof $\{D\}$. Therefore $\{D\}$ can replace $\{d\}$ in equations as long as the summation of all $[k]$ and $\{r_e\}$ is performed to obtain $[K]$ and $\{R\}$, respectively. $[K]$ is assembled by adding each element stiffness matrix $[k]$ such that it affects only its own same dof in the global matrix $[K]$. The global load vector can be formed in the same way. Now the potential energy can be expressed as

$$\Pi_p = \frac{1}{2} \{D\}^T [K] \{D\} - \{D\}^T \{R\} \quad [15]$$

where $[K] = \sum_{n=1}^{numel} [k]_n$ and $\{R\} = \{P\} + \sum_{n=1}^{numel} \{r_e\}_n$

The principle of minimum potential energy states that the admissible configurations of a conservative system that satisfies the equations of equilibrium make the potential energy stationary with respect to small admissible variations of displacements. Π_p is a function of $\{D\}$, so applying the principle

$$\left\{ \frac{\partial \Pi_p}{\partial D} \right\} = \{0\}$$

yields $[K]\{D\}=\{R\}$

This matrix equation is a set of algebraic equations to be solved for $\{D\}$.

2.2. Nonlinear Analysis

In linear analysis the displacements are directly proportional to the loads. In such analysis it is assumed that the displacements and rotations are small and that the loads maintain their original directions as the structure deforms. In a linear analysis $[K]$ and $\{R\}$ from equation [5] are independent of the displacements $\{D\}$, whereas in nonlinear analysis $[K]$ and/or $\{R\}$ are functions of the displacements $\{D\}$ ¹⁰ Nonlinear analysis is more difficult because the principle of superposition does not apply; results cannot be scaled in proportion to load or combined to obtain different load cases.

Nonlinearities can be classified as material and geometric nonlinearities. Material nonlinearity is associated with changes in material properties, e.g., plasticity. Geometric nonlinearity is associated with large displacement and rotation. Other nonlinearities can be introduced when changing the boundary conditions and modeling contact problems.

Nonlinear problems cannot be solved in a single step. Algorithms are used to solve the problem by taking a series of linear ‘small’ steps. Each step linearly approximates a portion of the nonlinear solution. The tentative solution after each step is updated and iterated again until a convergence criteria is satisfied, when the next step’s solution is attempted and so on⁹

A single-dof system is used to discuss the various algorithms available. The discussion of this algorithm is independent of the type of nonlinearity and also applies to multi-dof nonlinear systems. The system is represented by a nonlinear spring subjected to a force P at one of the ends. As the spring is stretched -- u is increased -- the stiffness of the spring, represented by k , changes in a nonlinear fashion. The purpose of the analysis is to solve for the stretch u as a function of the load P . The spring stiffness k is a function of u and can be calculated for any value of u . To resemble the multi-dof equations $[K]\{D\}=\{R\}$, the assumption that the equation $ku=P$ cannot be solved explicitly for u as a function of P has to be made.

2.2.1. Newton-Raphson Method

Figure 1 illustrates the Newton-Raphson solution method. The first step is to assume $u=0$ and obtain the initial tangent stiffness k_{t0} . Applying a load increment $\Delta P_1=P_1-0$ and solving the linear equation $k_{t0}\Delta u_1=\Delta P_1$,

$$k_{t0}\Delta u_1 = P_1 - 0$$

$$\Delta u_1 = \frac{P_1 - 0}{k_{t0}}$$

$$u_a = 0 + \Delta u_1$$

Point a is found in figure 1. Displacements at points A and a are equal. There is a force imbalance between the force P_1 at point A and the spring's resisting force at point a . P_1 is greater than the spring's resisting force $r_a=ku_a$ for a stretch of u_a . This difference,

$P_a - r_a = e_{PA}$, is used to drive the displacement to the correct value u_1 through iterations.

These iterations are performed while holding P_1 constant.

For the first iteration, tangent stiffness k_{ta} is used to solve for Δu in equation $k_{ta}\Delta u = e_{PA}$. Adding Δu to u_a the point A' is found. A new force imbalance exists between points A' and a' . At point a' tangent stiffness $k_{ta'}$ starts the second iteration, yielding point A'' , which is so close to point 1 that it is not discernible on the plot. Each iteration reduces the force imbalance. Iterations are performed until the value of the force imbalance satisfies a convergence criteria. The convergence criteria must be set such that the allowable tolerance produces a 'close enough' solution at reasonable cost of computation. Then, the force is increased to P_2 and point C is found. Following the same iteration process point 2 is approached. This method establishes several points on the P vs. u curve, that can be connected to approximate the actual curve. The Newton-Raphson method can be computationally expensive in multi-dof problems because the tangent stiffness matrix $[K_t]$ must be constructed and reduced for equation solving in every iteration.

2.2.2. Modified Newton-Raphson Method

This method uses the tangent stiffness matrix $[K_t]$ calculated at the outset of the load level step throughout all iterations in that load level¹⁰. The tangent stiffness matrix $[K_t]$ needs to be constructed and reduced only once for each load level. However, the number of iterations for each load level can increase significantly as can be seen in figure

2. The rest of the process is carried out in the same manner as in the Newton-Raphson method¹⁰

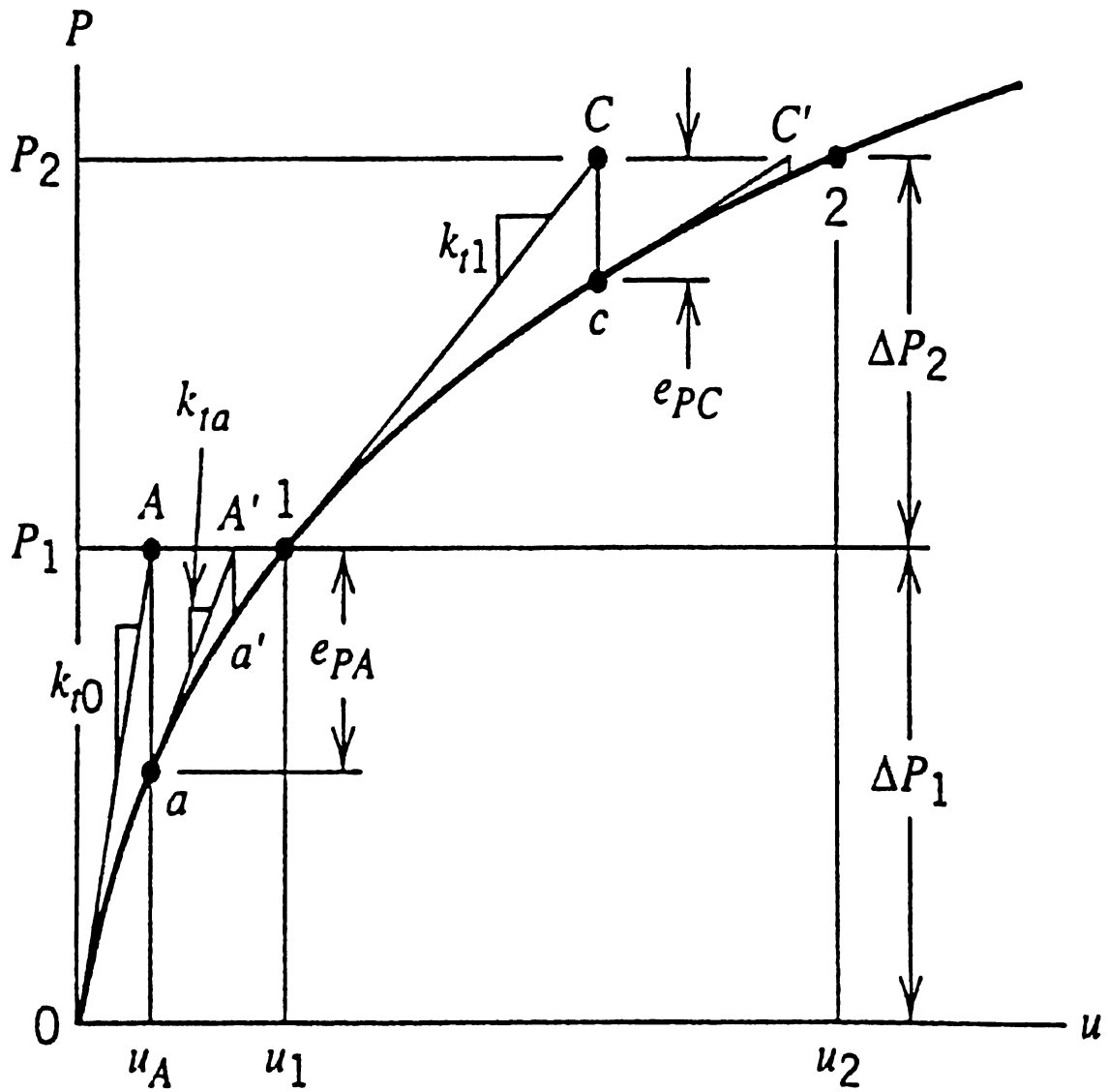


Figure 1. Newton-Raphson Incremental Solution¹⁰

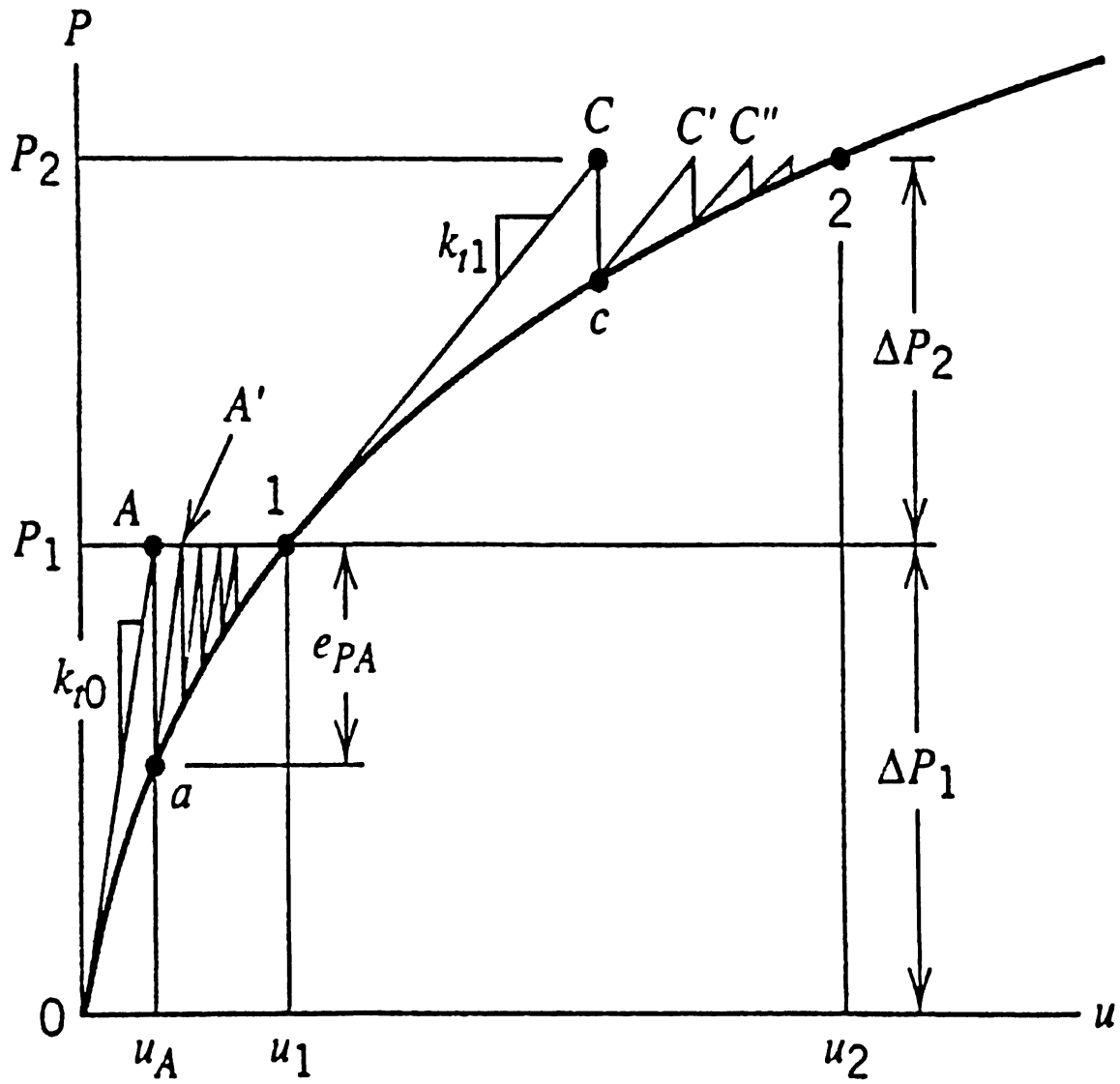


Figure 2. Modified Newton-Raphson incremental solution¹⁰

2.2.3. Contact Problem Overview

Modeling the contact interaction between structures requires information on the location of contact, areas of contacting surfaces and the solution for the surface tractions between structures in those areas. The analysis of a contact problem has to consider possible interference, sliding and loss of contact between structures in every event. The contact problem is by nature geometrically nonlinear¹¹. Figure 3 illustrates the contact interaction between two meshes. Parts 1 and 2 in figure 3a may make contact but it may not be known a priori, where on parts 1 and 2 contact will occur. An algorithm must

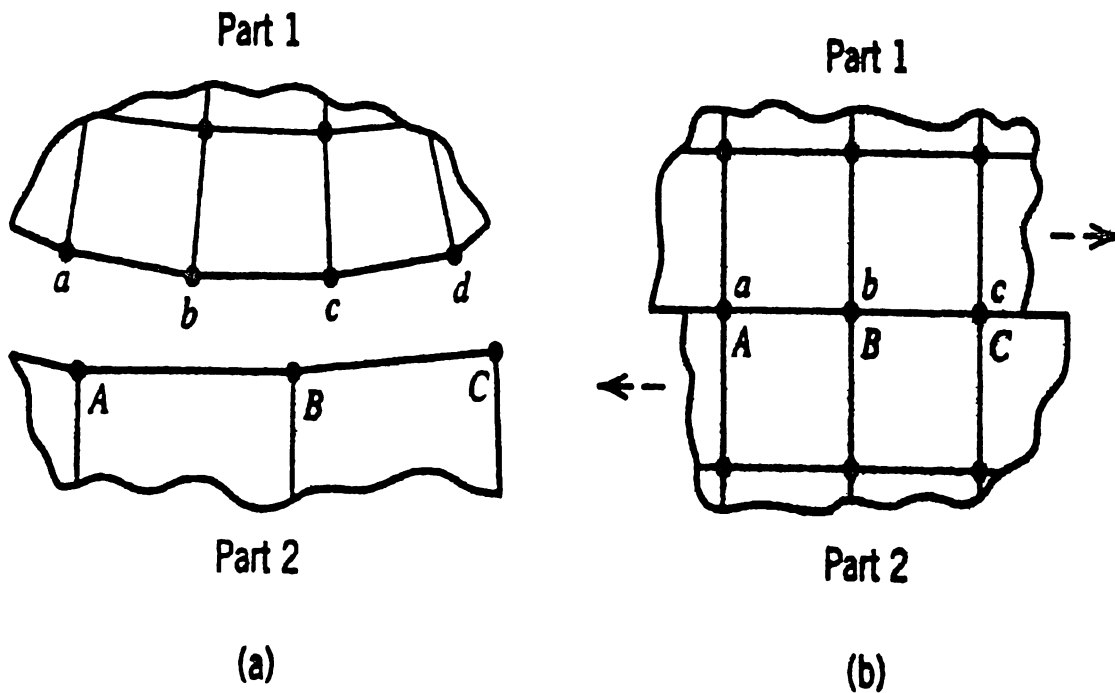


Figure 3. Two Meshes of a FE Model that (a) May come into contact, (b) Slide with respect to each other¹⁰

discover the contact location, prevent parts from penetrating each other and calculate their normal stresses. In figure 3b, parts 1 and 2 are already in contact, but it is not known how they will slide relative to one another. An algorithm must prevent sliding until friction is overcome, then calculate the shear force, at the same time allowing no tensile contact forces to develop.

Contact problems are problems of constraints. Algorithms have to constrain a node's dof against motion when it enters into contact with a fixed support, or they have to constrain a node's dof to have the same motion as an adjacent node when it comes into contact. There are two ways of imposing constrained conditions: Lagrange multipliers or the penalty method.

One way of approaching contact problems is by using gap-elements. These types of elements are defined at specific points (nodes) between contact surfaces, presetting the location of contact. Gap elements are formed by a bilinear spring and damping elements that act in the normal and tangential directions of contact surfaces, respectively¹². This element behaves differently in tension and compression. In tension, the surfaces are pulling away from each other, thus there is no stiffness. In compression the stiffness is set to an arbitrarily high number and is represented in the stress-strain curve by a straight line. The normal stress-strain relationship for gap elements is shown in figure 4a. The stiffness value K , must be selected such that closure of the gap can occur without allowing penetration¹².

The shear forces transmitted by the gap element correspond to the friction between the surfaces. The gap element allows the surfaces to slip only as long as the

shear stress is above a level determined by the analyst. The shear stress-strain relationship of a gap element is shown in figure 4b. Not choosing adequate stiffness values for the gap element in both the normal and tangential directions can create convergence problems in the solution¹⁰

Multiple-Point Constraint (MPC) can also be used to solve the load transfer problem between contacting surfaces in structural members. This method models contact

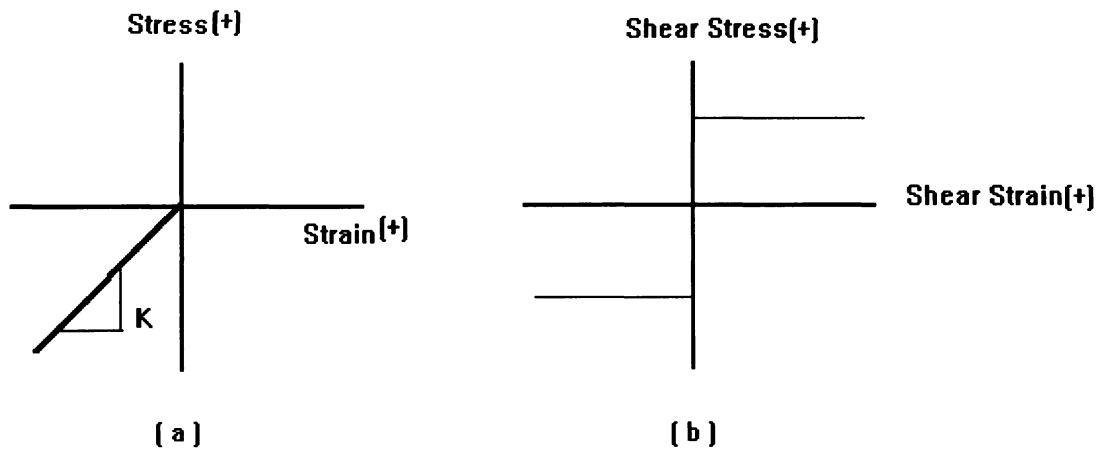


Figure 4. Stress-strain relationships for a gap element in the (a) normal direction, (b) tangential direction¹²

by coupling dof of adjacent nodes¹³. It requires that the points (nodes) of contact are known from the outset. The dof at these points are coupled so that the resultant force due to contact is normal to contacting surfaces. This means that the contact locations and contact directions must be predetermined, which in most problems is hard to do. Other

problems involving this approach is that the areas of contact must be assumed and friction cannot be modeled.

Some algorithms provide the flexibility of defining several potential contact conditions in terms of pairs of contacting surfaces. The analyst can define two sets of nodes or surfaces that may make contact¹³. One of the surfaces has to be defined as the 'master' surface and the other has to be defined as the 'slave' surface. The nodes on the 'slave' surface are constrained not to penetrate the master surface and the contact direction is always normal to the master surface¹³. The pressure-clearance relationship has to be defined so that the algorithm can determine when and where contact occurs and apply the required kinematic constraints to the respective set of nodes. Figure 5a shows a 'hard' contact pressure-clearance relationship. When the surfaces are in contact, any pressure stress can be transmitted between the surfaces. If the pressure reduces to zero, the surfaces separate. When the clearance becomes zero, the surfaces come into contact again. Another model of the pressure-clearance relationship is shown in figure 5b. It is called "softened" contact because, as the surfaces become in contact, the pressure increases exponentially. Contact between the surfaces occur when the clearance goes below the value of C .

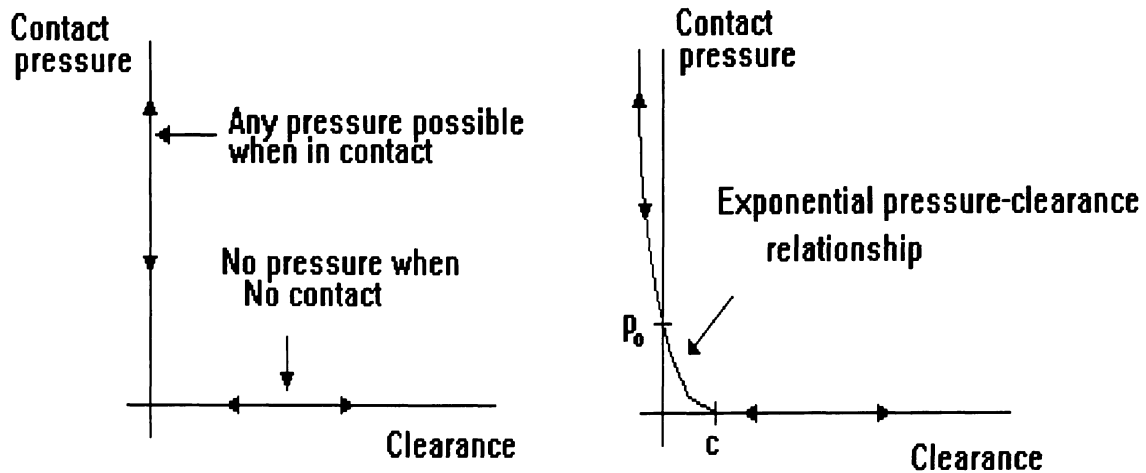


Figure 5. Pressure-Clearance relationship for (a) 'hard' contact, (b) 'softened' contact¹³

2.3. Dynamic Analysis

A structural problem is "quasistatic" if the frequency of the loading applied to a structure is approximately less than one-third of the structure's lowest natural frequency⁹. This means that if the loads are applied sufficiently slow, the problem can be treated as static and the $[K]\{D\}=\{R\}$ equation provides an adequate solution¹⁰. If the frequency of excitation is greater than one-third of the lowest natural frequency, inertia and damping effects cannot be neglected and a dynamic analysis is required.

Structural dynamics problems can be classified into two categories: modal analysis and time-history analysis. Modal analysis estimates the structure's natural frequencies of vibration and its mode shapes. The calculation of the natural frequencies is of major importance in the study of structural vibrations. If the frequency of excitation coincides with one of the natural frequencies of the system, a condition of resonance is

encountered and large oscillations result, leading to the catastrophic failure of the structure⁹ The time-history analysis provides the time varying response of the structure for a given loading The goal of this analysis is to solve for displacements, velocities and accelerations as a function of time

In structural dynamics problems the virtual work done by external forces has to be equal to the virtual work done by internal, inertial and viscous forces The expression for this virtual work principle for a single element is

$$\int_{V_e} \{\delta u\}^T \{F\} dV + \int_{S_e} \{\delta u\}^T \{\Phi\} dS + \sum_{i=1}^n \{\delta u\}_i^T \{P\}_i = \int_{V_e} (\{\delta \varepsilon\}^T \{\sigma\} + \{\delta u\}^T \rho \{\ddot{u}\} + \{\delta u\}^T k_d \{\dot{u}\}) dV \quad [16]$$

where $\{\delta u\}$ and $\{\delta \varepsilon\}$ are, respectively, small arbitrary displacements and their corresponding strains, $\{F\}$ is the body force, $\{\Phi\}$ is prescribed surface traction, $\{P\}_i$ are concentrated loads that act at a total of n points (nodes) on the element, $\{\delta u\}_i^T$ is the virtual displacement of the point at which load $\{P\}_i$ is applied, ρ is the mass density of the material, and k_d is a material damping parameter analogous to viscosity

For a given displacement field $\{u\}$, the velocity and acceleration vectors are

$$\{u\} = [N]\{d\} , \quad \{\dot{u}\} = [N]\{\dot{d}\} , \quad \{\ddot{u}\} = [N]\{\ddot{d}\} \quad [17]$$

The shape functions $[N]$ are functions of space and the nodal dof $\{d\}$ are functions of time. Inserting equation [17] into equation [16] yields

$$\{\delta d\}^T \left\{ \int_{V_e} [B]^T \{\sigma\} dV + \int_{V_e} \rho [N]^T [N] dV \{\ddot{d}\} + \int_{V_e} k_d [N]^T [N] dV \{\dot{d}\} - \int_{V_e} [N]^T \{F\} dV - \int_{S_e} [N]^T \{\Phi\} dS - \sum_{i=1}^n \{P\}_i \right\} = 0 \quad [18]$$

Since $\{\delta d\}$ is arbitrary, equation [18] can be written as

$$[m]\{\ddot{d}\} + [c]\{\dot{d}\} + \{r^{int}\} = \{r^{ext}\} \quad [19]$$

where the element's mass and damping matrices are defined as

$$[m] = \int_{V_e} \rho [N]^T [N] dV$$

$$[c] = \int_{V_e} k_d [N]^T [N] dV$$

and the element's internal force and external load vector are defined as

$$\{r^{int}\} = \int_{V_e} [B]^T \{\sigma\} dV = [k]\{d\}$$

$$\{r^{ext}\} = \int_{V_e} [N]^T \{F\} dV + \int_{S_e} [N]^T \{\Phi\} dS + \sum_{i=1}^n \{P\}_i$$

Equation [19] is the governing equation for structural dynamics for a single element. It states that externally applied loads $\{r^{ext}\}$ are resisted by the sum of the three internal forces: stiffness forces $\{r^{int}\}=[k]\{d\}$, damping forces $[c]\{\dot{d}\}$ and inertia forces $[m]\{\ddot{d}\}$. This equation is a system of coupled second order ordinary differential equations, and it represents a finite element “semidiscretization” because, although displacements $\{d\}$ are discrete functions of space, they are still continuous functions of time. It is discretized in time by the use of direct integration methods, which provide a sequence of simultaneous algebraic equations.

The governing structural dynamic equation for the assembled structure is given by

$$[M]\{\ddot{D}\} + [C]\{\dot{D}\} + [K]\{D\} = \{R^{ext}\} \quad [20]$$

The structure matrices $[M]$, $[C]$ and $[K]$ are constructed by expanding the element matrices $[m]$, $[c]$ and $[k]$ to “structure size” as explained in previous sections. $\{R^{ext}\}$, in general, contains the external loads applied as a function of time. This equation represents the dynamic response of the whole structure.

2.3.1. Damping

“Internal friction” in the material and slip in the connections of structures are mechanisms of dissipation of energy or damping⁹ They cause the amplitude of free vibration to decay in time. Sources of damping are not viscous and are difficult to represent mathematically. Damping forces $[C]\{\dot{D}\}$ are less than roughly 10% of forces $[K]\{D\}$, $[M]\{\ddot{D}\}$, and $\{R\}$ in equation [20]. These forces are small enough that they can be idealized as viscous, by the use the damping scheme called Rayleigh or proportional damping¹⁰

The damping matrix $[C]$ is formed as a linear combination of the stiffness and mass matrices,

$$[C] = \alpha[K] + \beta[M] \quad [21]$$

where α and β are called the stiffness and mass proportional damping constants. The relationship between α , β and the damping ratio ξ at frequency ω is given by

$$\xi = \frac{1}{2} \left(\alpha\omega + \frac{\beta}{\omega} \right) \quad [22]$$

Values of ω_1 , ω_2 , ξ_1 , ξ_2 are chosen by the analyst. ω_1 is the lowest natural frequency and ω_2 is chosen as the highest frequency of interest. Typical values for ξ range from 0.02 for piping systems to about 0.07 for bolted structures¹⁰ Once the two sets of values for ω and ξ are chosen, they are substituted into equation [22] and the resulting two equations are solved to obtain α and β .

2.3.2. Direct Integration Methods

Direct integration methods are used to solve the governing structural dynamics equation [20]. These methods replace the time derivatives in equation [20] by making a finite difference approximation of the displacement $\{D\}$ at time increments⁹

The dynamic response equation is written in the form

$$[M]\{\ddot{D}\}_n + [C]\{\dot{D}\}_n + [K]\{D\}_n = \{R^{ext}\}_n \quad [23]$$

where subscript n represents time $n\Delta t$, Δt is the size of the time increment and $\{R^{ext}\}_n$ is the known time dependent forcing function at instant n . For nonlinear problems, the matrix $[K]$ in equation [23] is a function of displacement as well as time. The goal is to solve for $\{D\}_n$, $\{\dot{D}\}_n$ and $\{\ddot{D}\}_n$ at particular instants of time.

Difference methods can be categorized as explicit or implicit. Explicit methods have the form

$$\{D\}_{n+1} = f(\{D\}_n, \{\dot{D}\}_n, \{\ddot{D}\}_n, \{D\}_{n-1}, \dots)$$

$\{D\}_{n+1}$ is determined based on information on displacement and time derivatives of displacements at time $n\Delta t$ and before. Implicit methods have the form

$$\{D\}_{n+1} = f(\{\dot{D}\}_{n+1}, \{\ddot{D}\}_{n+1}, \{D\}_n, \dots)$$

$\{D\}_{n+1}$ is determined based on the time derivatives of $\{D\}_{n+1}$, which are unknown. Direct integration methods produce an equation of the form

$$[A]\{D\}_{n+1} = \{F(t)\} \quad \text{or} \quad \{D\}_{n+1} = [A]^{-1}\{F(t)\}$$

in which $[A]$ is nonsingular and independent of time in linear problems, while $\{F\}$ is a function of time. The specific form of $[A]$ and $\{F\}$ depend on each particular algorithm.

2.3.2.1. Central Difference Method

This is a popular explicit direct integration method. It uses a set of finite difference formulas to define velocity and acceleration at an instant n . $\{D\}_{n+1}$ and $\{D\}_{n-1}$ are expanded using Taylor series about time $n\Delta t$:

$$\{D\}_{n+1} = \{D\}_n + \Delta t\{\dot{D}\}_n + \frac{\Delta t^2}{2}\{\ddot{D}\}_n + \frac{\Delta t^3}{6}\{\dddot{D}\}_n + \dots \quad [24]$$

$$\{D\}_{n-1} = \{D\}_n - \Delta t\{\dot{D}\}_n + \frac{\Delta t^2}{2}\{\ddot{D}\}_n - \frac{\Delta t^3}{6}\{\dddot{D}\}_n + \dots \quad [25]$$

Terms containing Δt^3 and higher powers are discarded. The velocity is approximated by subtracting equations [24] and [25] and the acceleration is approximated by adding equations [24] and [25],

$$\{\dot{D}\}_n = \frac{1}{2\Delta t} (\{D\}_{n+1} - \{D\}_{n-1}) \quad [26]$$

$$\{\ddot{D}\}_n = \frac{1}{\Delta t^2} (\{D\}_{n+1} - 2\{D\}_n + \{D\}_{n-1}) \quad [27]$$

combining equations [26], [27] and [23] provides

$$[A] = \frac{1}{2\Delta t}[C] + \frac{1}{\Delta t^2}[M]$$

$$F(t) = [R] - \left[[K] - \frac{2}{\Delta t^2}[M] \right] \{D\}_n - \left[\frac{1}{\Delta t^2}[M] - \frac{1}{2\Delta t}[C] \right] \{D\}_{n-1}$$

At any instant n , $\{D\}_{n+1}$ is calculated from known values of $\{D\}_n$ and $\{D\}_{n-1}$. Velocities and accelerations are calculated from equations [26] and [27]. Initial displacements $\{D\}_0$ and velocities $\{\dot{D}\}_0$ are known. To estimate $\{D\}_1$, $\{D\}_{-1}$ needs to be known. $\{D\}_{-1}$ is determined using the following equation

$$\{D\}_{-1} = \{D\}_0 - \Delta t \{\dot{D}\}_0 + (\Delta t)^2 \frac{\{\ddot{D}\}_0}{2}$$

where $\{\ddot{D}\}_0$ can be determined from equation [23].

The central difference method is conditionally stable: for a Δt too large, the solution tends to diverge⁹. The stability limit is closely related to the time required for a stress wave to cross the smallest element in the model, so the time increment can be very short if the mesh contains small elements or if the stress wave speed in the material is very high¹³. To guarantee numerical stability

$$\Delta t < \Delta t_{cr} \quad \text{where} \quad \Delta t_{cr} = \frac{2}{\omega_{\max}} \equiv \frac{T_{\min}}{\pi}$$

where ω_{\max} is the largest undamped natural frequency of the system.

2.3.2.2. Newmark Method

The Newmark method provides the necessary numerical damping to high frequency oscillations. The basis of the method is the following set of equations

$$\{D\}_{n+1} \approx \{D\}_n + \Delta t \{\dot{D}\}_n + \frac{\Delta t^2}{2} \{(1-2\beta)\{\ddot{D}\}_n + 2\beta \{\ddot{D}\}_{n+1}\} \quad [28]$$

$$\{\dot{D}\}_{n+1} \approx \{\dot{D}\}_n + \Delta t \{(1-\gamma)\{\ddot{D}\}_n + \gamma \{\ddot{D}\}_{n+1}\} \quad [29]$$

where β and γ are numbers that can be chosen by the analyst to provide the desired stability and accuracy of the solution. A popular choice, called the “trapezoidal rule,” is $\gamma=1/2$ and $\beta=1/4$. Substitution of equations [28] and [29] into equation [23] yields

$$[A] = \frac{4}{\Delta t^2}[M] + \frac{2}{\Delta t}[C] + [K] \quad [30]$$

$$\{F(t)\} = \{R^{ext}\}_{n+1} + [M] \left\{ \frac{4}{\Delta t^2} \{D\}_n + \frac{4}{\Delta t} \{\dot{D}\}_n + \{\ddot{D}\}_n \right\} + [C] \left\{ \frac{2}{\Delta t} \{D\}_n + \{\dot{D}\}_n \right\} \quad [31]$$

$\{D\}_{n+1}$ is calculated from known values of $\{D\}_n$, $\{\dot{D}\}_n$, and $\{\ddot{D}\}_n$ by substituting equations [30] and [31] into $\{D\}_{n+1} = [A]^{-1}\{F(t)\}$. Equations [28] and [29] are used to calculate $\{\dot{D}\}_{n+1}$ and $\{\ddot{D}\}_{n+1}$, respectively.

The Newmark method is unconditionally stable when $2\beta \geq \gamma \geq \frac{1}{2}$ is satisfied. No matter how large Δt is, the solution converges¹⁰. This does not mean that the results are guaranteed to be accurate.

2.4. ABAQUS

ABAQUS is a commercially available general purpose finite element program designed for use in a wide variety of applications. The principal advantages of this program are its large library of capabilities, including a large element library and a wide range of nonlinear features. It also provides extensive output capabilities by the use of an interactive post-processor.

ABAQUS is capable of performing a wide variety of analyses, such as static analysis, eigenvalue buckling estimation, dynamic response analysis, eigenvalue extraction to calculate natural frequencies, heat transfer analysis, modal dynamic analysis, random response analysis, steady state dynamics and contact interaction analysis.

Designed for advanced applications, specifically in the nonlinear range, ABAQUS can also efficiently solve linear application problems. It is capable of dealing with three sources of nonlinearities: geometric nonlinearity, material nonlinearity and boundary nonlinearity. In nonlinear problems it is often difficult to obtain a convergent

solution at a low computational cost. ABAQUS uses the modified Newton-Raphson algorithm and offers an automatic convergence control approach, in which the user defines the step and the convergence criteria and ABAQUS automatically selects the increment size as it develops the response in the step. This approach allows nonlinear problems to be analyzed without extensive experience in the particular problem solution. Direct user control of the increment size is also available. This approach is good if the user has extensive knowledge about the solution response.

Nonlinear dynamic response problems are solved using direct integration methods. These methods are significantly more expensive than the modal methods used to solve linear problems. ABAQUS uses the Hilber-Hughes-Taylor operator, which is nothing but a slight modification of the Newmark method. This operator adds a parameter α to the Newmark equation that is used to introduce artificial damping in the system to allow the automatic time stepping procedure to work smoothly¹³. Structural damping is available by defining the stiffness and mass proportional damping constants in the Rayleigh damping equation. ABAQUS also provides an automatic incrementation scheme for use in dynamic analysis.

The user can analyze contact interaction problems using ABAQUS' "contact pair" approach, in which pairs of potential contact surfaces need to be defined as well as the pressure-clearance relationship between them. The algorithms automatically determine locations of contact and stress transmitted (normal and shear).

3. VALIDATION OF PASSENGER-SEAT INTERFERENCE

3.1. General

When subjected to decelerations, a seated passenger transmits inertia loads to the seat-restraint system. The interaction between the passenger and the seat-restraint system determines how the magnitude and direction of the inertia loads vary as a function of time. To accurately analyze the structural behavior of the seat in a crash scenario, it is required to model the dynamic response of the passenger and the means of transferring the inertia loads to the seat-restraint system.

The purpose of this chapter is to describe and validate the approach used to simulate the passenger-seat interaction under decelerative forces, using finite element modeling capabilities.

Output from the program SOM-TA is used for the validation. The output for a sample case run provides the time-history response of the passenger and the seat. The same case is modeled in ABAQUS and the results are compared. The models of the passenger (dummy), seat-restraint system and their interaction are discussed in the following sections.

3.2. Dummy Model Description

The aircraft passenger model used in this research is based on information obtained from the Anthropomorphic Test Dummy (ATD) defined in 49 CFR part 572 and the Hybrid III crash test dummy. The Hybrid III is a 50th percentile adult male crash

test dummy developed by General Motors Corporation in the 1970s. In 1986, The National Highway Traffic Safety Administration incorporated the Hybrid III into part 572 of the Federal Motor Vehicle standards¹⁴. The Hybrid III is now been used by all domestic and most foreign car manufacturers in vehicle development programs.

The purpose of this model is to simulate the mechanics and kinematics of the passenger throughout a crash event. It is not meant to represent any particular dummy, but a dummy that would approximately simulate the response of a passenger.

The three-dimensional dummy model is made up of twelve rigid links as shown in figure 6, which is a schematic representation of the model, identifying segments, centers of gravity and joints. The number of segments is the minimum that will permit accurate, meaningful simulation of a three dimensional response⁶. Hands and feet are included as part of the forearm and lower leg segments, respectively.

3.2.1. Model Segment Definition

The characteristics required to define each segment of the model are length, mass, center of mass location and moment of inertia. Model segment dimensions and characteristics were obtained from reference 6. This reference provides tables of the segment's characteristics for the part 572 ATD. The segments of the model are broken down as follows: lower legs (2), upper legs (2), lower torso, upper torso, upper arm (2), forearm (2), neck and head. The dummy segments are defined as rigid body elements. Each of these elements has a reference node that carries the element's kinematic

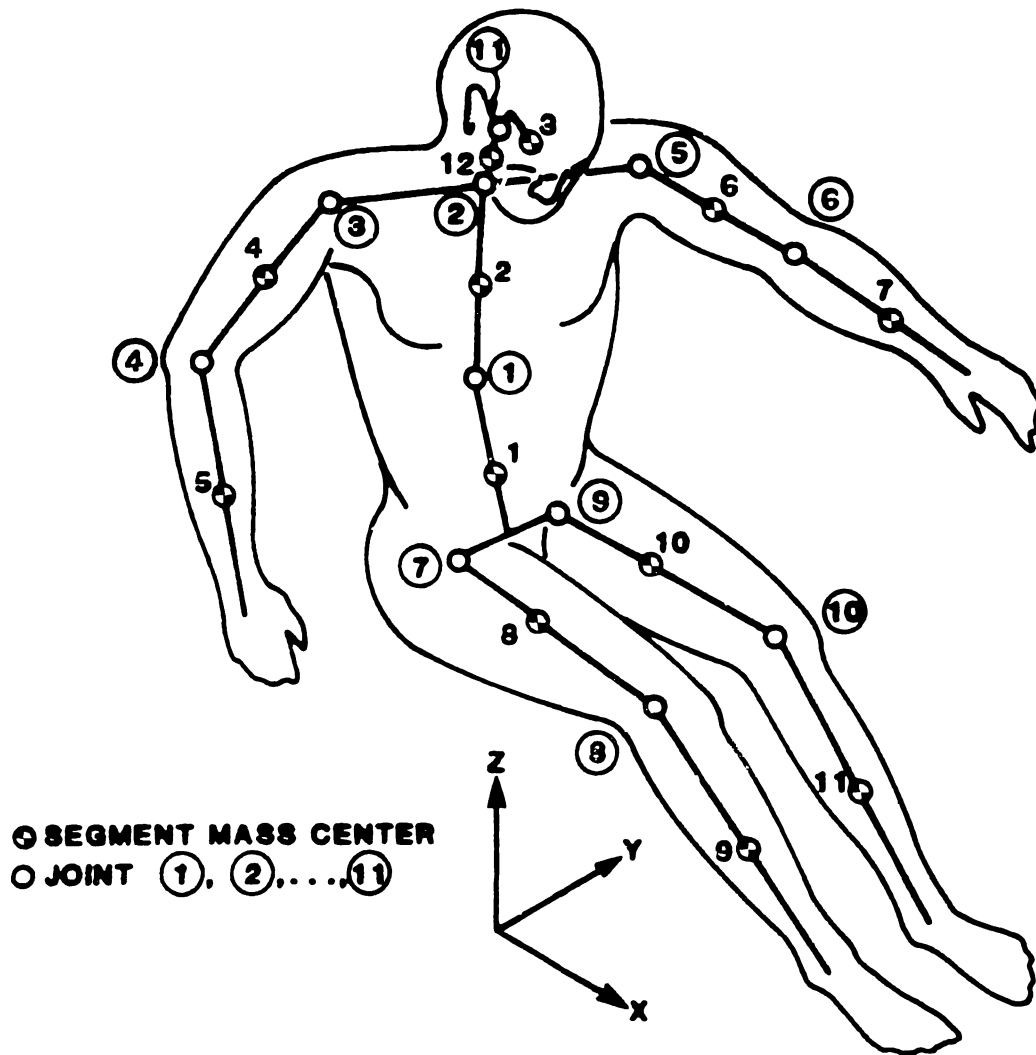


Figure 6. Three-Dimensional Representation of The Dummy Model.⁶

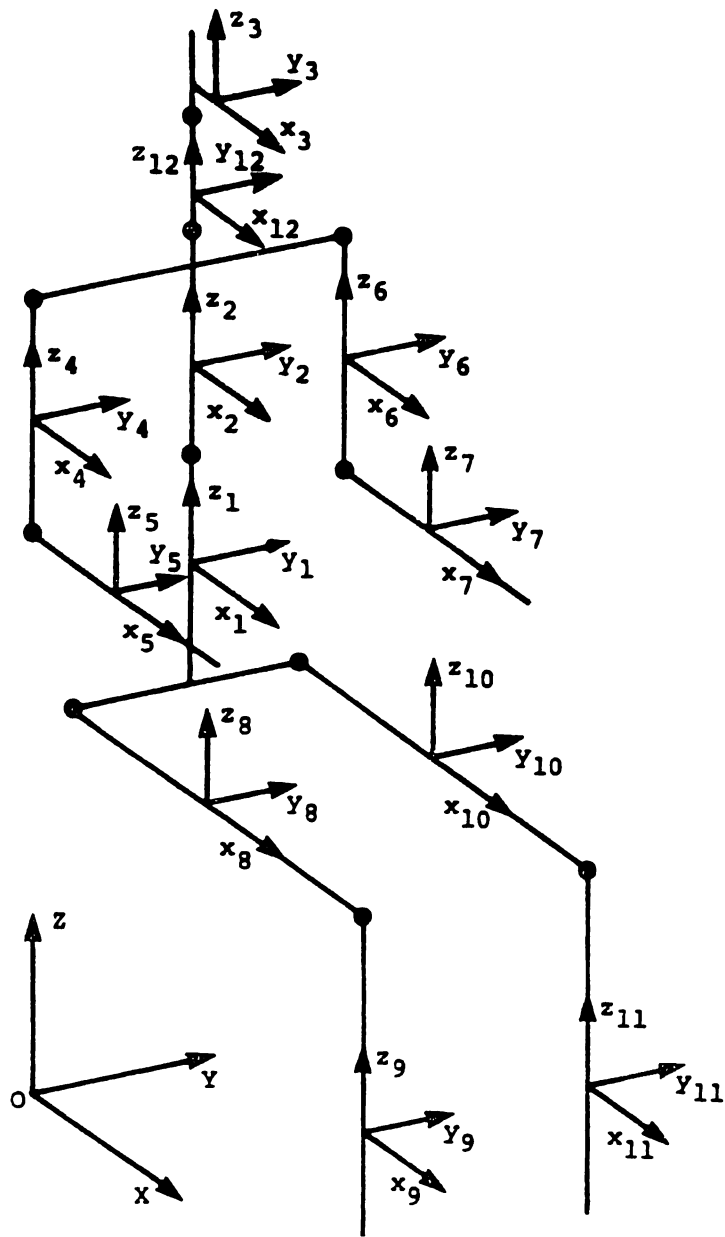


Figure 7. Rigid Elements Local Coordinate Systems.⁶

variables. The reference node is defined at the center of gravity of each segment. The length of the segment is defined as the distance between joint centers, rather than standard anthropometric dimensions based on external measurements. The line connecting the joints of each segment is assumed to be a principal axis of inertia. Thus, the moments of inertia are all principal. The mass of each element is defined as a lumped mass element at the center of gravity. A local rectangular coordinate system is defined at the center of gravity of each segment as shown in figure 7. These local coordinate systems are the principal axes of inertia of the elements and are used to define the principal moments of inertia. They rotate with the segments with respect to the global coordinate system.

3.2.2. Model Joint Characteristics

The model consists of 11 joints as shown in figure 6. The joints allow relative rotation of the segments with respect to each other. The allowed relative rotation (dof) in each joint depends upon the joint type. Resistive torque as a function of angle of rotation for the different joints of the Hybrid III dummy are provided in reference 15. The model contained herein uses the same joint characteristics as the Hybrid III.

A typical curve of joint resistance vs. angle of rotation is shown in figure 8. The free range motion is the interval where no resistance to rotation is exerted by the joint. Once the rotation of the joint exceeds the joint stop angle (θ_s) the resistive torque increases in a nonlinear manner with increasing angle of rotation¹⁵ The maximum

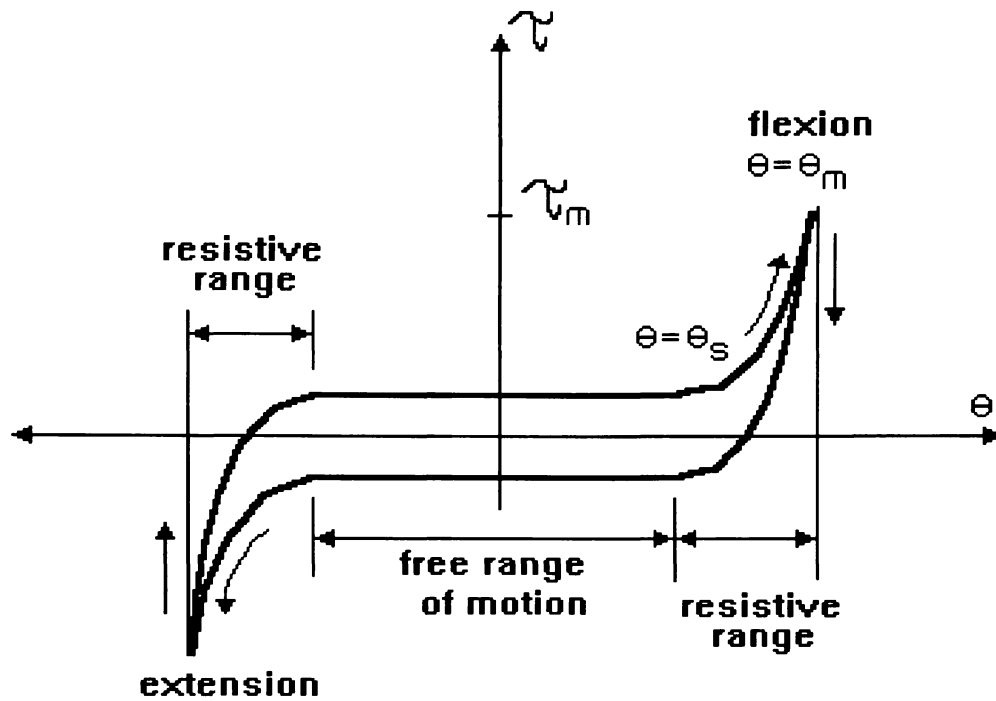


Figure 8. Illustration of typical joint test curve¹⁵

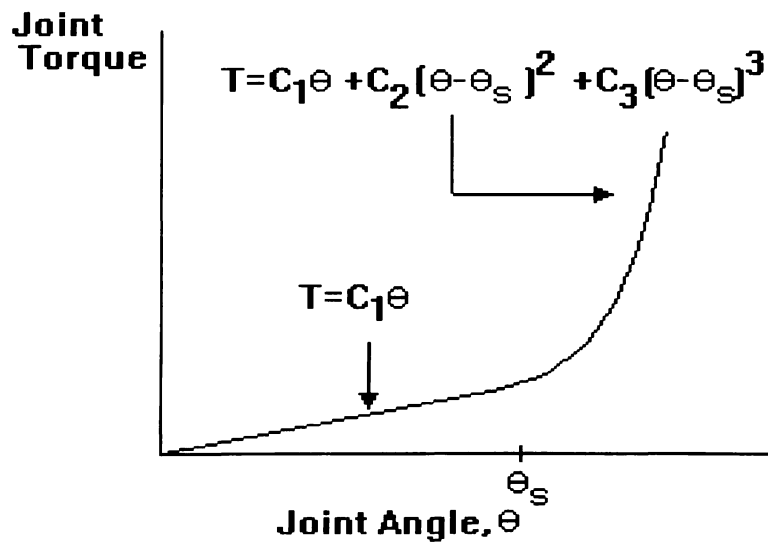


Figure 9. Joint torque approximation curve¹⁵

rotation of the joint is θ_m . The mechanical behavior of the joint is modeled using two curves as shown in figure 9. The linear part models the free range of motion. Some joints provide small muscular resistance in which case C_1 takes a non-zero value, otherwise, it takes the value of zero, as in, knee and elbow joints. C_2 and C_3 define the nonlinear resistive range of the joint.

Flexible joint elements in the ABAQUS element library are used to model the mechanics of the joints. These elements have 6 dof, allowing relative displacement (3 directions) and rotation (3 directions) of the segments attached to them. Internal stiffness and damping are created with the use of linear/nonlinear springs and dashpots. The behavior of the flexible joint element is defined in terms of a local rectangular coordinate system that rotates with one of the segments that connect to the joint. Segments of the dummy cannot translate with respect to each other. Therefore high stiffness linear springs are defined in the local x,y and z directions for all joints. Table 1 shows the different joints and their respective active degrees of freedom. Nonlinear torsional springs are used to define the resistive torque of all the joints using the approximation shown in figure 9. Damping in the joint is defined as constant and slightly below the critical damping coefficient¹⁴. Resistive torques of flexion-extension and adduction-abduction motions for the shoulder joint are coupled. This is not possible to model using the flexible joint element, so these two types of motion are modeled independently of each other.

The range of motion of the joints cannot be limited by just defining θ_m with the use of flexible joint elements. In ABAQUS, torsional spring stiffnesses are set to high enough values to prevent joints from rotating past the angle of maximum deformation.

Table 1. Degrees of freedom in joints of the dummy model.

Joint	degrees of freedom	type of motion
Knee	1	flexion-extension
Elbow	1	flexion-extension
Hips	2	flexion-extension, adduction-abduction
Spine	2	bending (forward and lateral)
Neck	3	bending (forward and lateral), torsion
Head	3	bending (forward and lateral), torsion
Shoulder	2	flexion-extension, adduction-abduction

3.3. Seat Model Description

Detailed information on this seat was obtained from a SOM-TA sample run. This seat represents a conventional airline coach-class passenger seat. An illustration of the model of this seat is shown in figure 10.

The two sets of legs are modeled using 4130 steel. Each set of legs consists of a rear, diagonal and front beam. The cross section of these beams are square and hollow with a wall thickness of 0.065 in. and width of 1.25 in. The attachment of both front and rear legs to the tracks prevents vertical, forward and transverse movement as well as rotation with respect to a vertical axis. The front legs are attached to the seat's front spar, and the rear and diagonal legs are attached to the seat's rear spar. These connections transfer all combinations of loads and moments.

ABAQUS

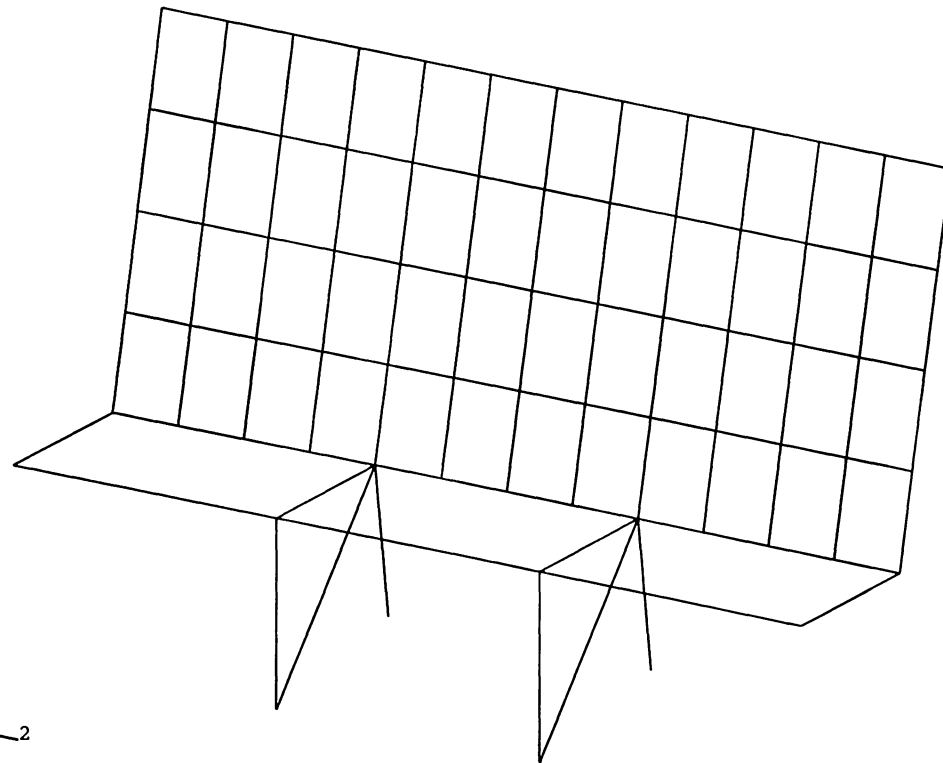


Figure 10. Three-Dimensional Sketch of the seat used for the validation

The two spars, front and rear, have a hollow circular cross-section of 1.75 in. outside diameter and 0.083 in. wall thickness. They are made of 2024-T4 aluminum alloy. Front and rear spars are connected by four cross-beams, which have the same cross-section as the legs, but are made of 2024-T4 aluminum. Spars, legs and cross-beams are modeled using beam elements. The seat back rests, although modeled, have no structural importance because they carry no load on forward-facing seats during a crash. The back rest is modeled using 0.1 in. thick aluminum plate elements. Seat belts are modeled using 0.1 in.² cross-sectional truss elements. The seat model consists of 229 elements, 204 nodes and 1224 degrees of freedom

3.4. Dummy-Seat Interaction

As the passenger model flails forward during a crash, it transmits inertia loads to the seat through the cushion and the seat belt. Buttocks and upper legs interact with the seat throughout the deceleration process. This interaction was modeled to take advantage of ABAQUS capabilities to model contact interference.

The seat cushion is not modeled due to lack of available information about its mechanical behavior. Moreover, it would significantly increase the number of dof and make the analysis computationally more expensive. Contact effects need to be modeled between the dummy upper legs (rigid line elements) and the pan of the seat (plate elements). ABAQUS does not support three dimensional contact interaction for one-dimensional element, i.e., the dummy's legs. The lower section of a cylinder is used to model the surface of the dummy's legs that enter into contact with the pan of the seat.

This surface is modeled using rigid plate elements and is constrained to translate and rotate with the rigid line elements that represent the upper legs of the dummy.

The approach used to solve the contact problem is the finite-sliding formulation. This algorithm allows separation and sliding of finite amplitude as well as arbitrary rotation between the contacting surfaces. The surface of the dummy's legs (rigid plate elements) are chosen as the 'master' surface and the pan of the seat is chosen as the 'slave' surface. The pressure-clearance relationship is defined as 'hard' and friction forces are taken into account in the analysis.

This type of analysis presented convergence problems. Overclosure (penetration) of the contacting surfaces at several points - after a few increments into the solution caused the solution to diverge. When interpenetration occurs beyond a certain overclosure limit, ABAQUS reduces the time increment size and re-iterates. Subsequent cutbacks in the time increment size made it go below the minimum time increment allowable for stability of the numerical time integration scheme. Both contacting surfaces were refined to no avail. The algorithm went a few increments further into the solution but the same problem occurred. The pressure-clearance relationship was changed to 'soft contact' It was thought that the 'hard' contact relationship was inducing excessively high stress gradients between the contacting surfaces, and this was contributing to the convergence problem. This change did not improve the outcome of the analysis.

Another contact formulation was tried to obtain a solution to the contact problem. The small-sliding contact algorithm allows the surfaces to undergo small sliding relative to each other, but they may undergo arbitrary rotation.

Sample auxiliary problems were used to get a better understanding of ABAQUS contact formulation. The problem of a sphere making contact with a plate was modeled. Convergence of the solution improved as the meshes were refined, but at a very slow rate. The time increments used by the algorithms were on the order of 10^{-7} seconds. This was computationally expensive and it had to be discarded. It is believed that the meshes of the contacting surfaces need to be extremely fine. However, that does not guarantee the convergence of the solution. It increases the number of dof and dramatically increases running time and storage requirements. The highly nonlinear nature of the solution and lack of experience dealing with this type of problem contributed to the modeling problems discussed here. Technical support from ABAQUS is not available under academic license.

A simpler and more computationally effective approach to modeling contact effects is to use Multiple-Point Constraints (MPC). Vertical beam elements are fixed to the legs of the dummy at two different points, as shown in figure 11. The lower ends of these beams are constrained to have the same vertical displacement as the seat pan. They are also constrained to have the same rotations as the seat pan with respect to vertical axis 3 in figure 11. The passenger is constrained to slide forward by the seat pan and belt. The stiffness of the beam elements is chosen to be an arbitrary large number, such that the stress in the element is negligible compared to the stress in the seat belt. This type of approach does not provide a thorough analysis of the interaction between the seat and the dummy, but it provides a solution to the load transfer problem.

ABAQUS

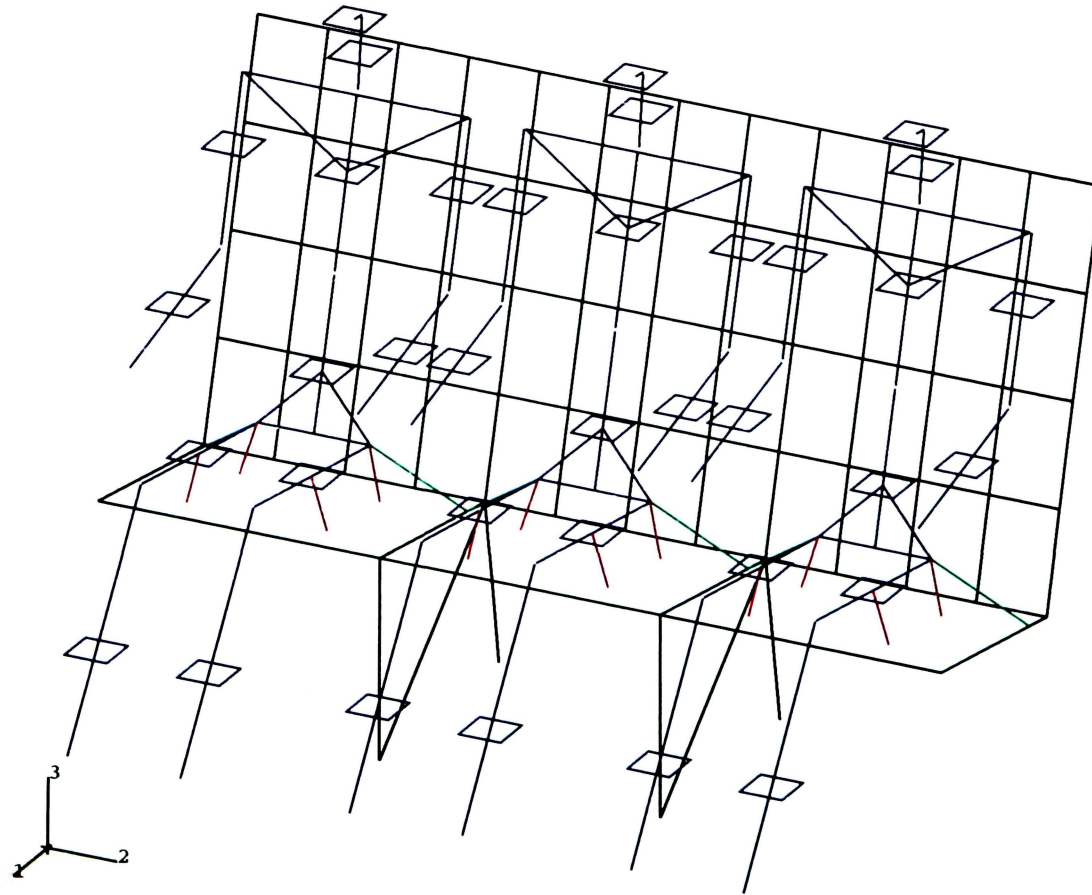


Figure 11. Passenger/Seat Model Representation

The entire model is shown in figure 11. It consists of 360 elements, 390 nodes and the stiffness matrix has 1734 dof. Dummy models are drawn in blue, the seat is drawn in black, seat belts are shown in green and the “interference-beam elements” are drawn in red.

Two nonlinear analyses were performed with the model. In a static nonlinear analysis, the left front leg of the seat was subjected to a downward displacement of 0.5 in. Then, a nonlinear dynamic analysis was used to subject the entire model to a forward inertia load. The load varies in a trapezoidal fashion. It increases linearly from 0 to 6g in 0.01 seconds, remains at 6g until 0.155 seconds have passed and, then decreases linearly to 0 in a matter of 0.01 seconds. ABAQUS was used to perform these analyses.

3.4. Analysis of Results

To establish structural damping coefficients, an eigenvalue estimation of the natural frequencies was performed on the seat model. The first natural frequency was thereby estimated as 27.27 rad/s. The frequency range of interest was set between the first natural frequency ω_1 , and the forcing frequency ω_2 . Damping ratios ξ_1 and ξ_2 were set to 0.02 and 0.029, respectively⁹. Having these parameters set, Rayleigh damping is introduced in the seat model by calculating the values for the proportional damping constants, α and β . Using equation [20b], $\alpha=0.047$ and $\beta=0.0014$.

The seat belt force varied in the same oscillatory fashion as SOM-TA's, but the amplitude was considerably higher. With this initial estimation of structural damping

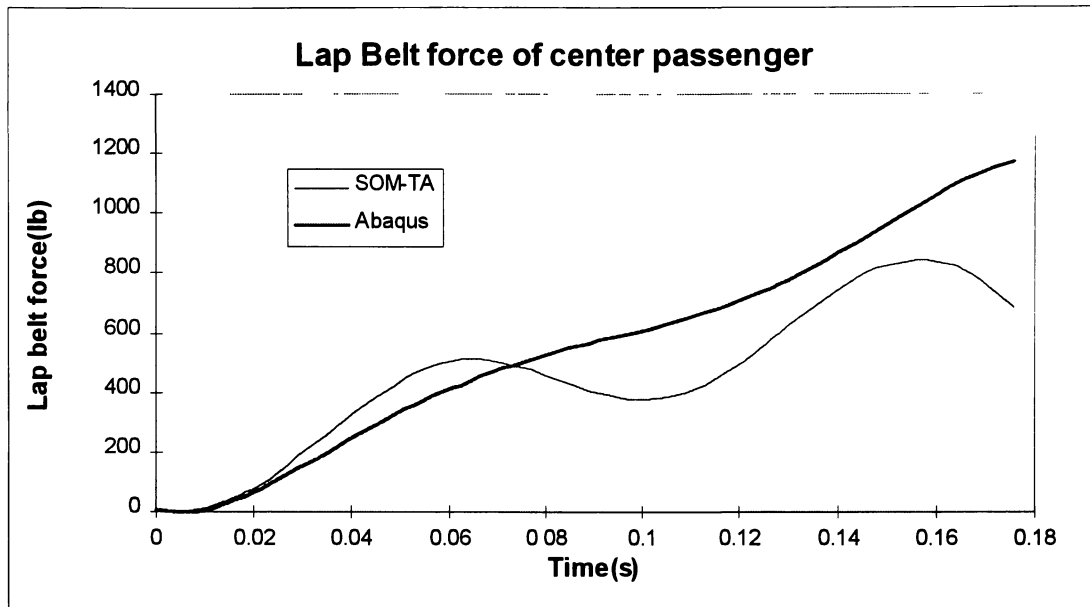


Figure 12. Lap Belt Force Comparison between ABAQUS and SOM-TA Model

Response.

effects, the maximum force was 2400 lb, which is 3 times higher than that predicted by SOM-TA. This is attributed to the approach used to model the interaction between the dummy and the seat. Friction cannot be modeled when using multiple-point constraint. Thus, the dummy can slide freely with respect to seat pan, thereby exerting a larger force on the seat belt. The proportional damping constants of the seat belt were varied in an effort to reduce the amplitude of the response and fit SOM-TA's seat belt curve. Changes in the mass proportional damping constant β did not affect the response. As the stiffness proportional damping constant α , was increased, the amplitude decreased, but the curve 'flattened' out. The value of α was increased to find the best approximation to SOM-TA's seat belt response. The best approximation was found for $\alpha=0.08$. The seat belt force curve is shown in figure 12. After 0.07s ABAQUS approximation is consistently

higher than SOM-TA's but within the same order of magnitude. The biggest discrepancy between both curves is 500 lb and occurs at 0.176 s.

The overall reaction of the dummy to decelerative forces can be seen in figures 13 and 14. The X axis is horizontal and the Z axis is vertical. As expected, the C.G. of the dummy displaces forward (increase in X direction) and down (decrease in Z direction) when subjected to forward deceleration. The displacement of the dummy's C.G in the X-direction (figure 13) is always higher than the one predicted by SOM-TA, with the greatest difference being 1.5 inches at 0.176 s. In the Z-direction (figure 14) the greatest difference is 1.25 inches, also at 0.176 s. However, the trend of the response in the Z-direction does not match SOM-TA's as well as it does in the X-direction. The C.G. of the ABAQUS dummy moves up in the first 0.09 s. SOM-TA's dummy C.G. does the opposite, moving downward. It is believed that this is because the SOM-TA model included the seat cushion. As the passenger flails forward, the legs apply pressure on the cushion and compress it, further lowering the location of the passenger's C.G. in the vertical axis. The ABAQUS dummy model estimates the location of the C.G. of the dummy to within 1.5 inches compared to SOM-TA. Lateral displacement (Y-direction) of the dummy due to forward deceleration is negligible.

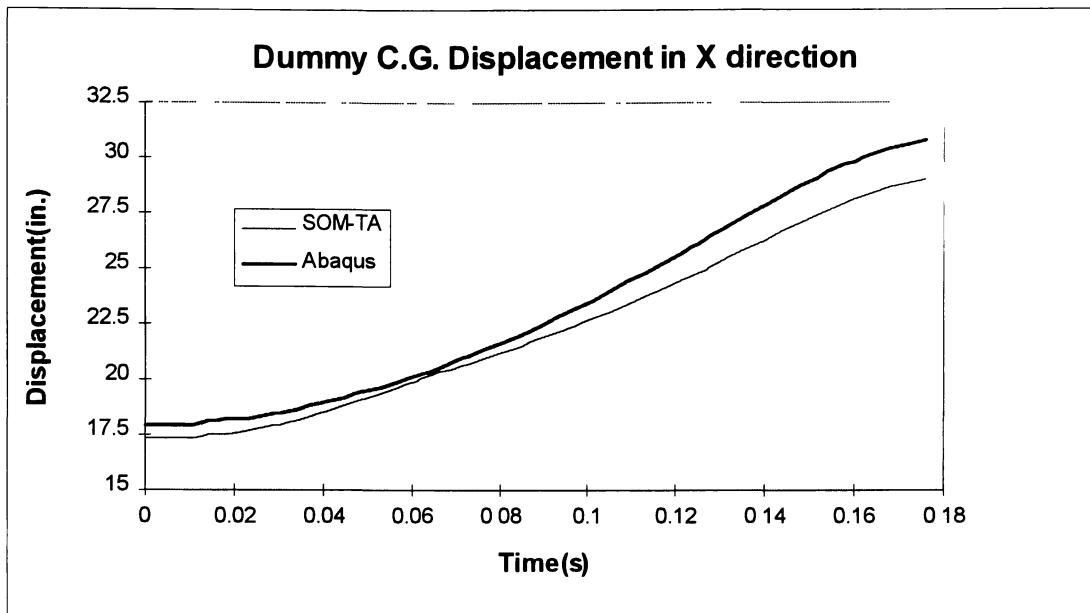


Figure 13. Time-History response of the dummy with respect to the X axis compared to SOM-TA's.

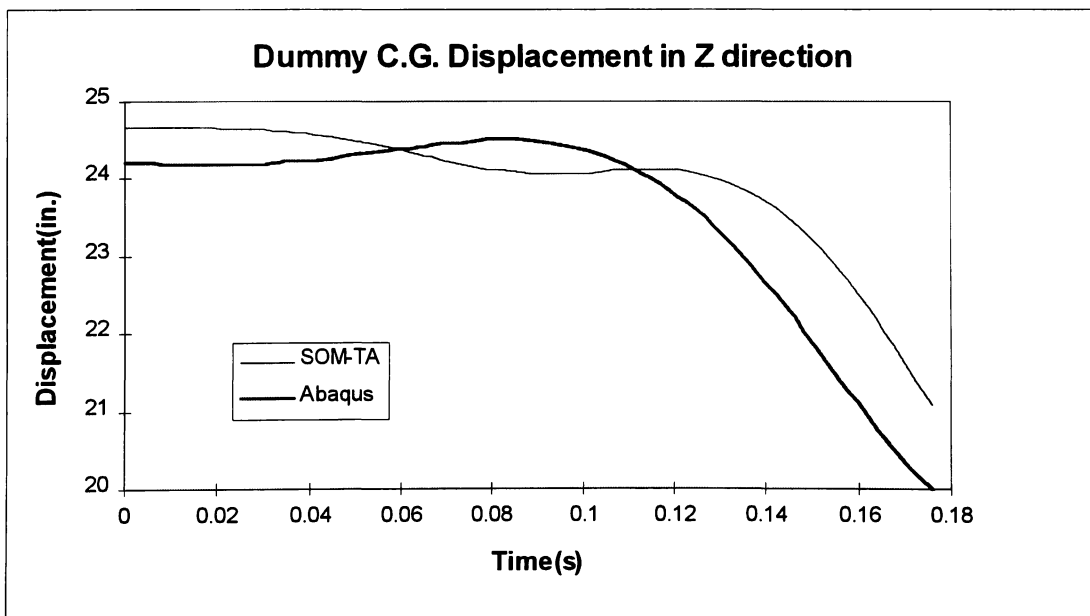


Figure 14. Time-History response of the dummy with respect to the Z axis compared to SOM-TA's.

A comparison of ABAQUS seat model response against SOM-TA's predicted seat deformation is presented in tables 2 and 3. These tables show the displacements of characteristic nodes of the seat in the X, Y and Z axes at two different time intervals.

Figure 15 shows the location of the nodes in the seat structure. Most of the displacements predicted by ABAQUS are within 20 to 25 percent difference compared to SOM-TA.

The biggest percent difference, 64% ,is present at $t=0.025$ sec. in node 38 in the Z

Table 2. Seat model displacement comparison in the X,Y and Z axis at $t=0.025$ sec.

NODE	X-Direction			Y-Direction			Z-Direction		
	SOM-TA	Abaqus	%Diff	SOM-TA	Abaqus	%Diff	SOM-TA	Abaqus	%Diff
7	0.351	0.3556	1	-0.1808	-0.1474	18	-0.0595	-0.0672	13
19	0.4125	0.4085	1	-0.1343	-0.1055	21	-0.4992	-0.5054	1
26	0.0047	0.0035	25	-0.1806	-0.1508	17	0	0.0001	0
38	0.007	0.0060	15	-0.1348	-0.1163	14	-0.0009	-0.0015	64
39	0.6355	0.5878	8	-0.1339	-0.1032	23	-0.7619	-0.7111	7
61	-0.1037	-0.1222	18	-0.1344	-0.1182	12	0.244	0.2361	3
62	0.5627	0.5231	7	-0.1811	-0.1464	19	-0.2722	-0.1830	33
84	-0.1011	-0.1074	6	-0.1806	-0.1518	16	0.2309	0.1348	42

Table 3. Seat model displacement comparison in the X,Y and Z axis at $t=0.175$ sec.

NODE	X-Direction			Y-Direction			Z-Direction		
	SOM-TA	Abaqus	%Diff	SOM-TA	Abaqus	%Diff	SOM-TA	Abaqus	%Diff
7	0.3573	0.3605	1	-0.1733	-0.1396	19	-0.0576	-0.0655	14
19	0.4222	0.4161	1	-0.1296	-0.0961	26	-0.5005	-0.5069	1
26	0.0112	0.0085	25	-0.1714	-0.1431	17	0.002	0.0020	3
38	0.0166	0.0137	18	-0.1321	-0.1091	17	-0.0023	-0.0029	25
39	0.9195	0.8384	9	-0.1276	-0.0860	33	-0.9336	-0.8796	6
61	0.1937	0.1229	37	-0.1346	-0.1112	17	0.0204	0.0259	27
62	0.7935	0.7495	6	-0.1744	-0.1353	22	-0.1285	-0.1268	1
84	0.1576	0.1048	34	-0.1677	-0.1451	13	0.3191	0.1695	47

direction. All the nodes of the seat modeled in ABAQUS deform in the same direction as the seat modeled in SOM-TA. All displacements predicted by ABAQUS in Y-direction are smaller than those predicted by SOM-TA. Therefore, the ABAQUS seat model is more rigid in the lateral direction.

The seat stress response is linear throughout the dynamic step. Failure by material yielding did not occur. The member that was exposed to the highest stress was the left front leg, as can be seen in figure 16, which shows contours of the Von-Mises Failure criteria throughout the seat structure at $t=0.223$ sec. The maximum Von-Mises stress of 63,044 psi occurred at the connection between the left front leg and the front spar. This stress level is below the yielding stress with a margin of safety of 1.53. The asymmetrical response of the seat is due to the 0.5 in. downward displacement initially applied to the left front leg.

ABAQUS

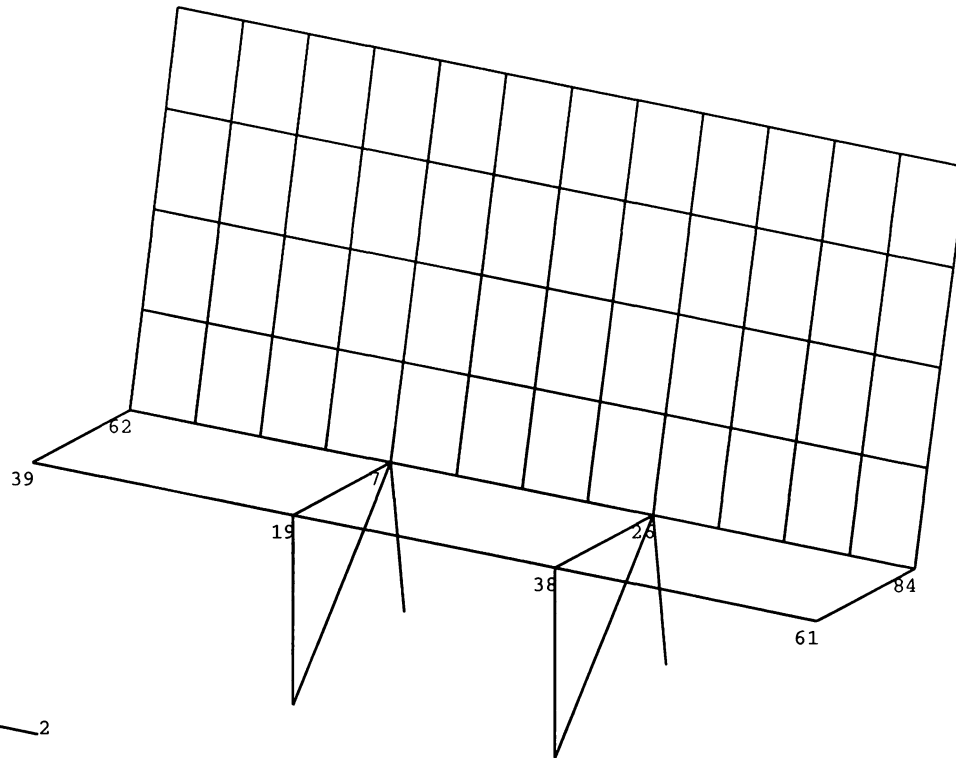


Figure 15. Illustration of Particular Nodes in the Seat Structure

ABAQUS

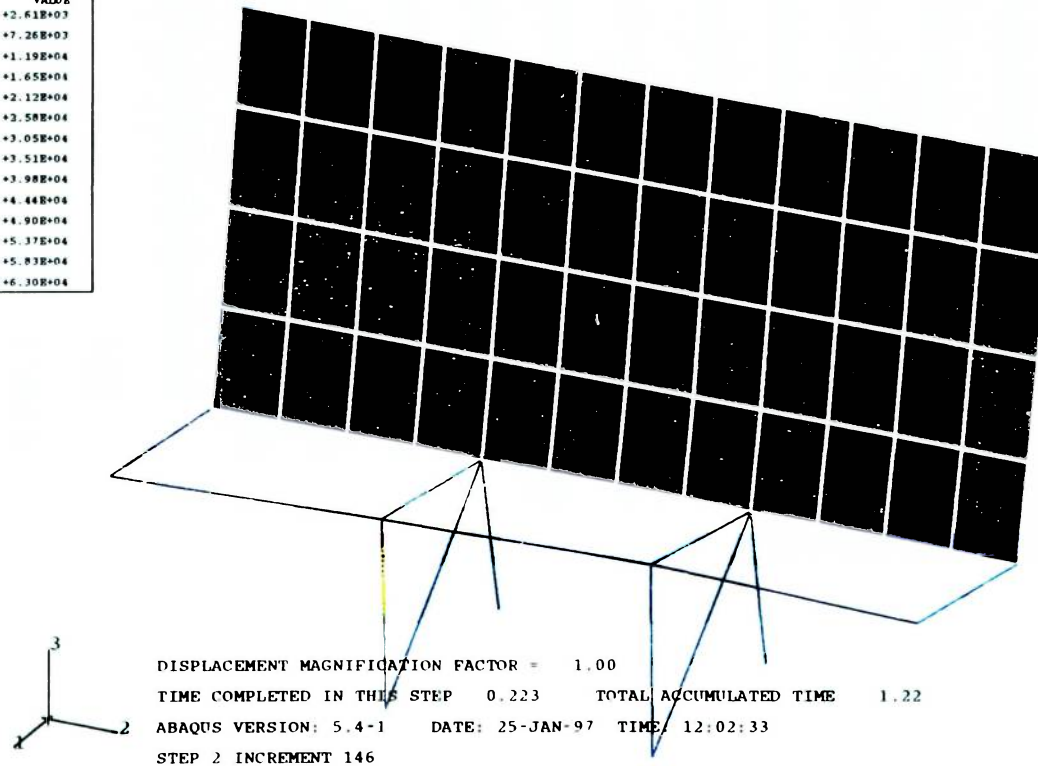
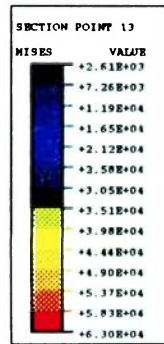


Figure 16. Von-Mises Failure Criteria at $t=0.223$ s.

4. ENERGY-ABSORPTION SEAT DESIGN

4.1. Design Considerations

The proposed seat design must be able not only to withstand the dynamic tests as stated by the certification criteria but also to absorb some of the impact energy. The seat must move forward to reduce the inertia forces experienced by the passenger⁴. However, it must deform in a controlled manner. Total deformation on the seat must be enough to absorb impact energy, but not to the extent of impeding evacuation of passengers. The seat must be designed to be fairly rigid in the lateral direction⁴. Large deformation in this direction would block the aircraft's aisle.

Geometric and material information on energy-absorbing seats available in the market was not possible to obtain. This type of information is considered proprietary by seat manufacturers. There is no established procedure for designing a passenger seat to varying loading conditions. For this project, several seats were designed and subjected to simulated dynamic tests in order to predict their performance and to determine if they could withstand the dynamic loading. They were tested using ABAQUS as a simulation tool. Changes from one seat to another were predominantly made in the seat legs. Member cross-sections, geometry, joint characteristics and support at the seat tracks were the parameters changed. Trial and error was used until a particular seat was able to pass the simulated dynamic tests.

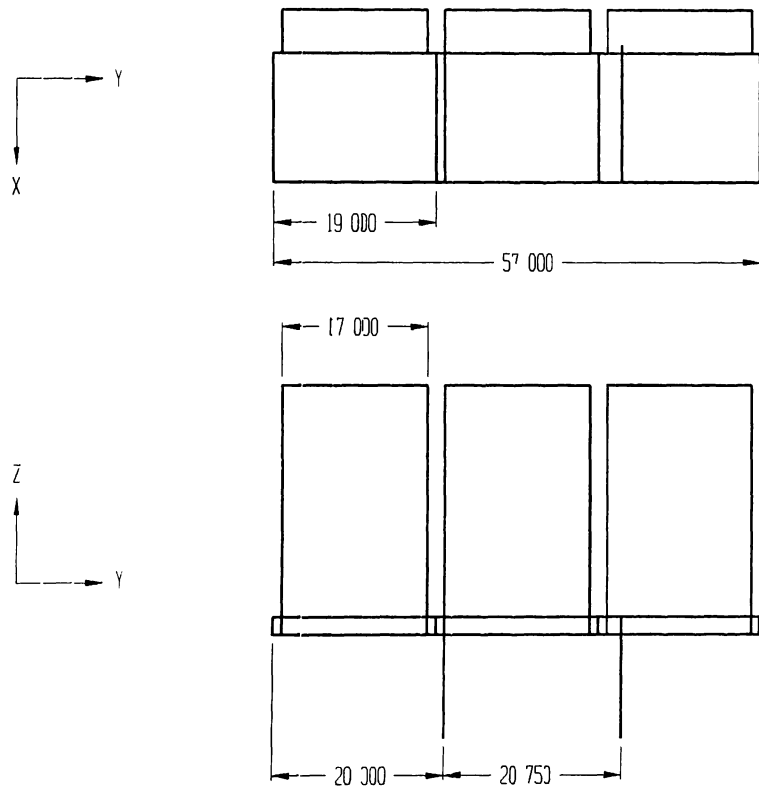
The most severe dynamic test is the misaligned 16g forward test. The deformations imposed on the seat tracks prior to dynamic loading expose the seat legs to

high levels of deformation and therefore high stresses. Attachment points at the seat tracks and beam connections in the seat allow some play and relieve some of the stresses. This is very complicated to model using finite element analysis. Some of the seat designs withstood the downward 14g loading and showed good energy-absorption capabilities, but failed to pass the 16g forward test. Stresses in the legs were far into the plastic range after the tracks were misaligned. The highest stresses were present in the legs attached to the track with 10 degrees of roll deformation.

In short, seats must be flexible enough to allow large deformations, yet must be rigid enough to withstand the prescribed dynamic loading and leave enough volume to permit passenger egress.

4.2. Energy-Absorbing Seat Description

This seat is designed to be used as a coach-class passenger seat in large transport aircraft. Figures 17,18 and 19 show element dimensions and cross-sections of the seat model. All seat structural members except the energy-absorber are made of 2024-T4 aluminum alloy. The rear legs have a square, hollow cross-section that tapers as it approaches the seat tracks. Rear leg attachments to the seat tracks provide no resistance to rotation about the X and Y axes. Their connections to the rear frame transmits all loads and moments. Front legs are modeled as truss elements and their attachments to the tracks prevent transverse (Y) and vertical (Z) displacements. Front and rear legs are connected



All dimensions are in inches

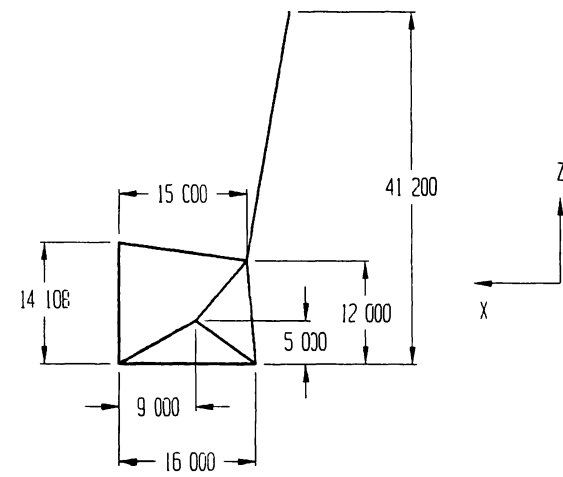


Figure 17. Dimensional Layout of Energy-Absorbing Seat

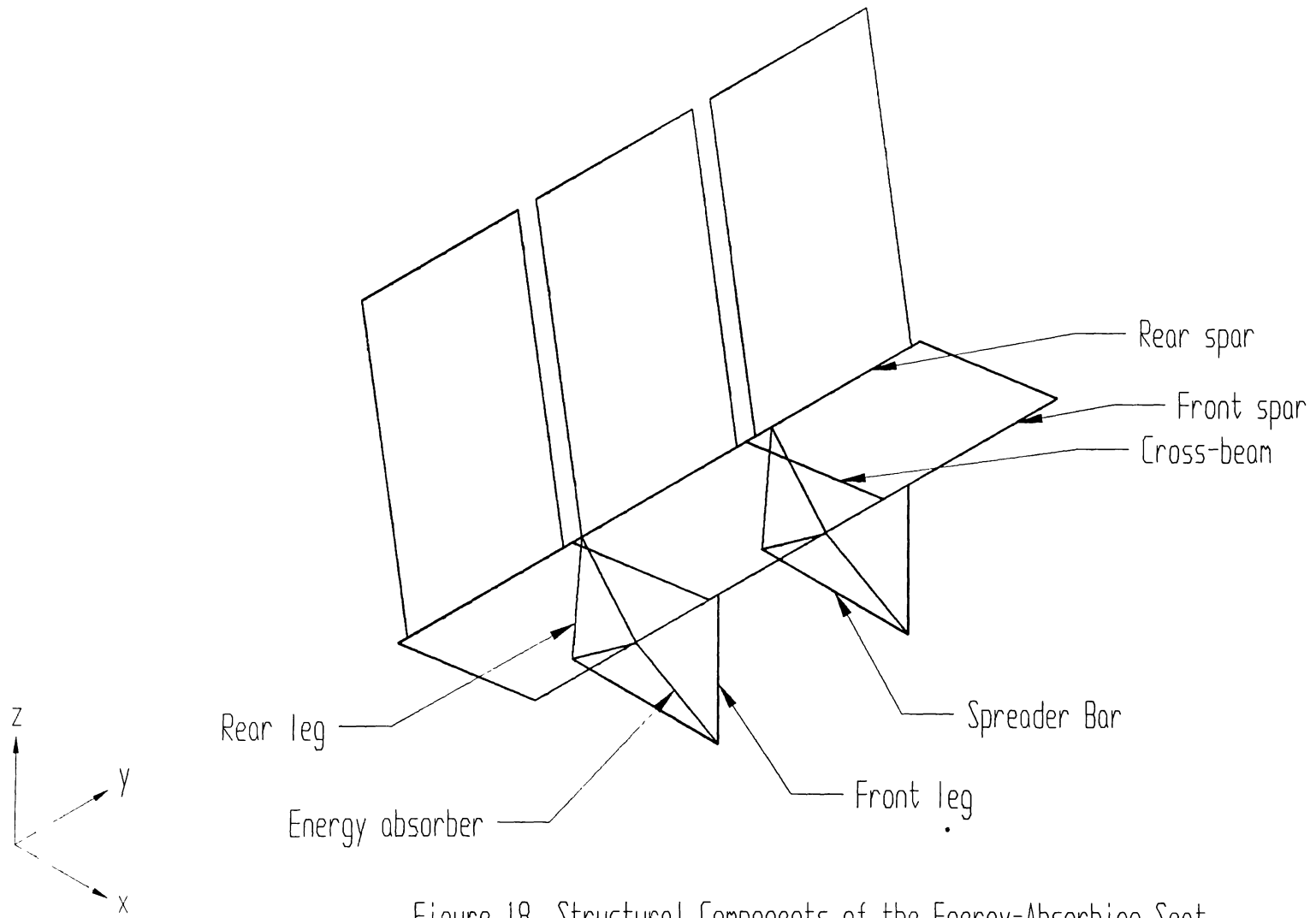
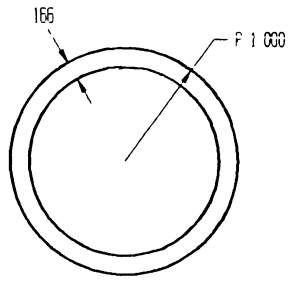
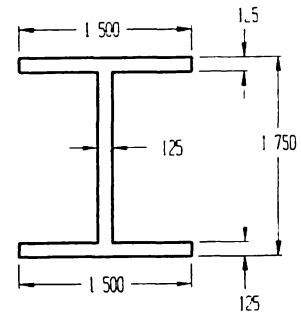


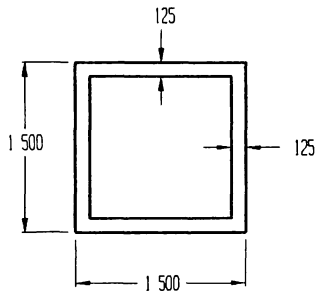
Figure 18. Structural Components of the Energy-Absorbing Seat



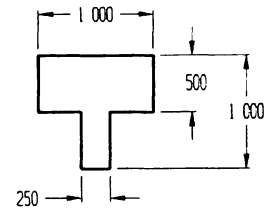
Front and rear spar cross-section



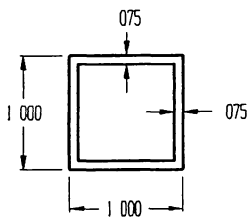
Cross-beams I-section



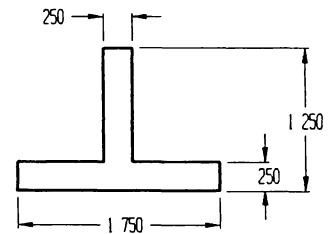
Rear legs cross-section



Diagonal beams T-section



Front legs cross-section



Spreader leg cross-section

All dimensions are in inches

Figure 19. Cross-sections of Structural Members of the Seat

by the spreader bars just above the seat track. They are modeled as two-force members and prevent movement of the front legs along the seat tracks. Diagonal beams connect the energy-absorber with both ends of the rear legs. Both diagonal beams have a T-shaped cross-section. Their connection to the rear legs transmits all loads and moments. The front and rear 'spars' are connected by four I-section cross beams. Cross beam attachments to the spars allow rotation with respect to the longitudinal axis of the spars. Although the seat backs are modeled, they have no effect in the performance of the seat. Both leg assemblies are shifted to the right (toward the aisle of the aircraft) to allow for installation in the aircraft. Dimensions of the leg separation and placement with respect to the spars were obtained from actual measurements during commercial flights.

The behavior of the materials used in the seat structure is defined in the linear and nonlinear ranges to allow for plastic deformation. Material strain rate dependency is neglected. The ultimate strength of aluminum 2024 subjected to dynamic impact of 25 ft/sec is 68 ksi¹⁶. This increase in strength is considered negligible compared to the ultimate static strength of 65 ksi.

The device used to absorb the energy is the inversion tube energy absorber. It works under tension and compression loads only. As loads are applied at both ends, a length of the inner metal tubing is turned inside-out or outside-in (plastically deforming that section) depending on the type of loading¹⁷. This process limits the load by continuously deforming the new material up to the particular point in the stress-strain curve. Figure 20 shows a sketch of the inversion tube energy absorber and its load-

deflection characteristic. The energy absorbers are modeled using truss elements. The materials used in the actual inversion tube are 3003-H14 aluminum and mild steel.

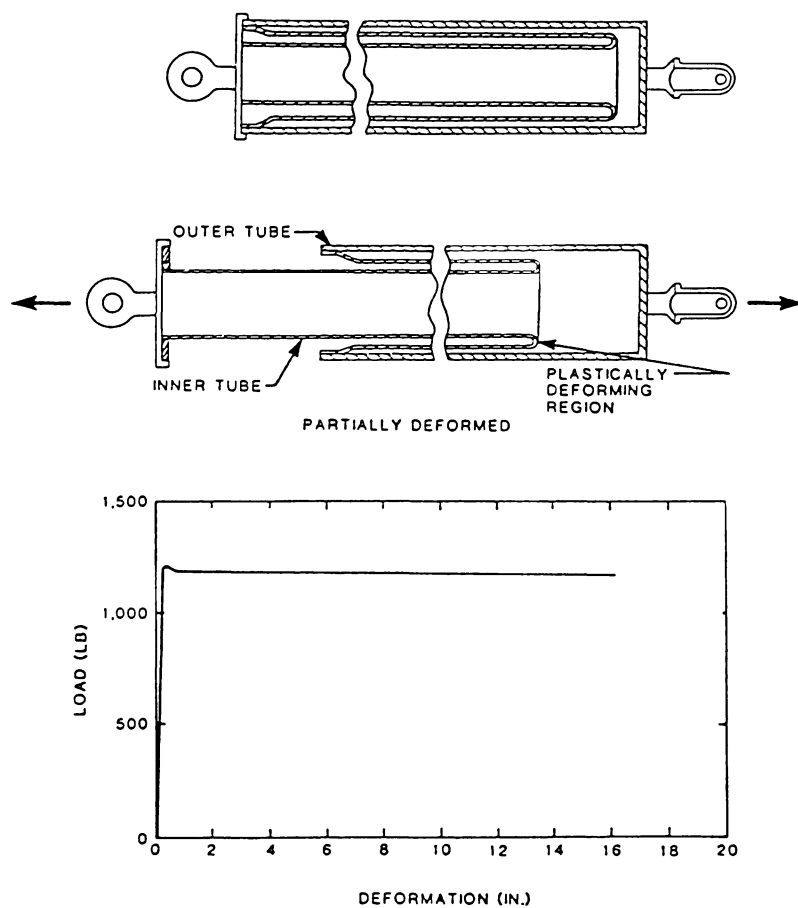


Figure 20. Inversion Tube Load-Deflection characteristics.¹⁷

4.3. Dynamic Test Simulation Results of the Energy-Absorbing Seat

The first test causes the seat tracks to deform in the pitch (Y) and roll (X) axes and induces a forward 16g floor deceleration. A nonlinear static step analysis is performed to apply this prescribed initial displacement. The attachment point of the seat's right leg assembly is displaced according to the 10 degree vertical track deformation. Seat track fittings allow free rotation of the seat legs in the roll direction. Therefore, ten degree displacement of the left track does not impose any type of loading on those attachment points.

The deformation of the track induced a Von-Mises stress of 44,008 psi on the lower diagonal beam member of the right set of legs of the seat and is shown in figure 21. This stress is the highest in the structure and has exceeded the 44 ksi yielding stress of the material. Plastic deformation occurs in both of the energy absorbers. The stresses in these members reach the load limiting value of 41,600 psi.

The 16g forward (X) floor deceleration is applied as a 16g forward gravitational load on the passenger and the seat. Maximum forward deformation of the seat occurs at $t=0.170$ s. Figure 22 shows a contour plot of the forward displacement of the seat at this time. The deformation shown in this figure is relative to the initial position. Due to the vertical deformation of the track and the asymmetric loading, the seat undergoes a small rotation with respect to the vertical axis. Forward displacement of the right section of the seat is greater than the left side. This forward deformation is thought to be small enough as to not obstruct passenger egress. The seat is relatively rigid in the lateral direction. It deforms away from the aircraft's aisle.

ABAQUS

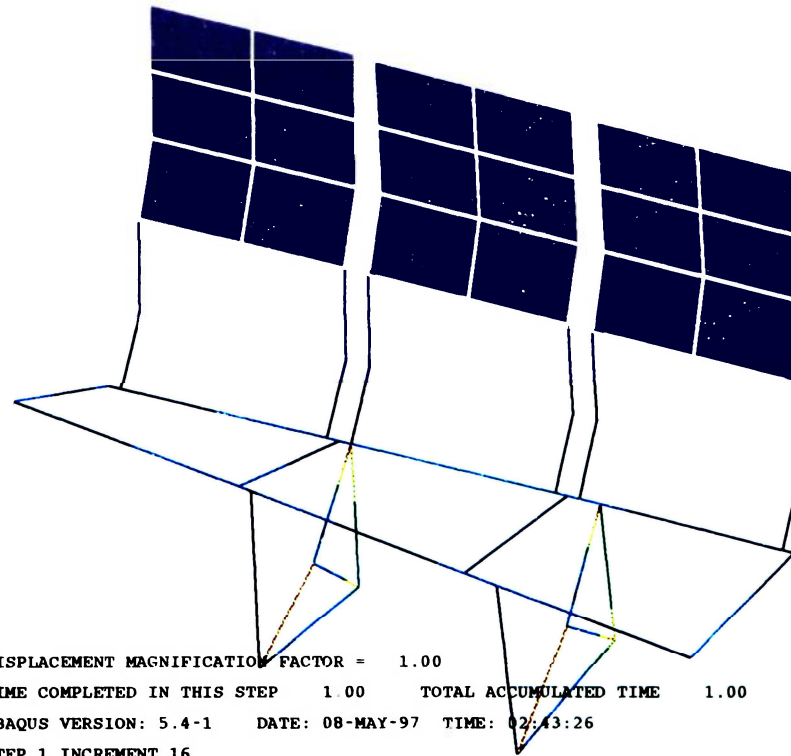
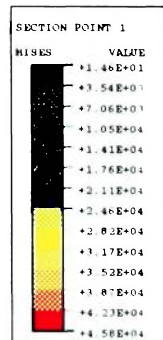


Figure 21. Von-Mises Failure Criteria after seat track deformation

ABAQUS

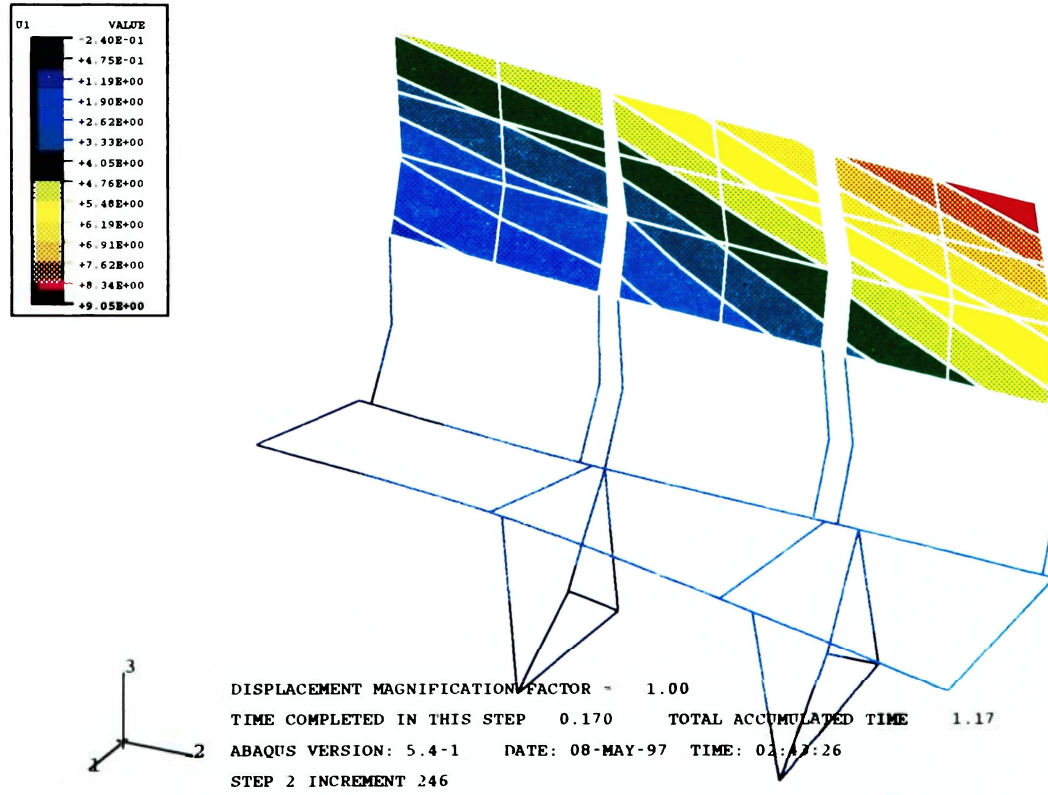


Figure 22. Forward Seat Deformation at $t=0.170$ s.

ABAQUS

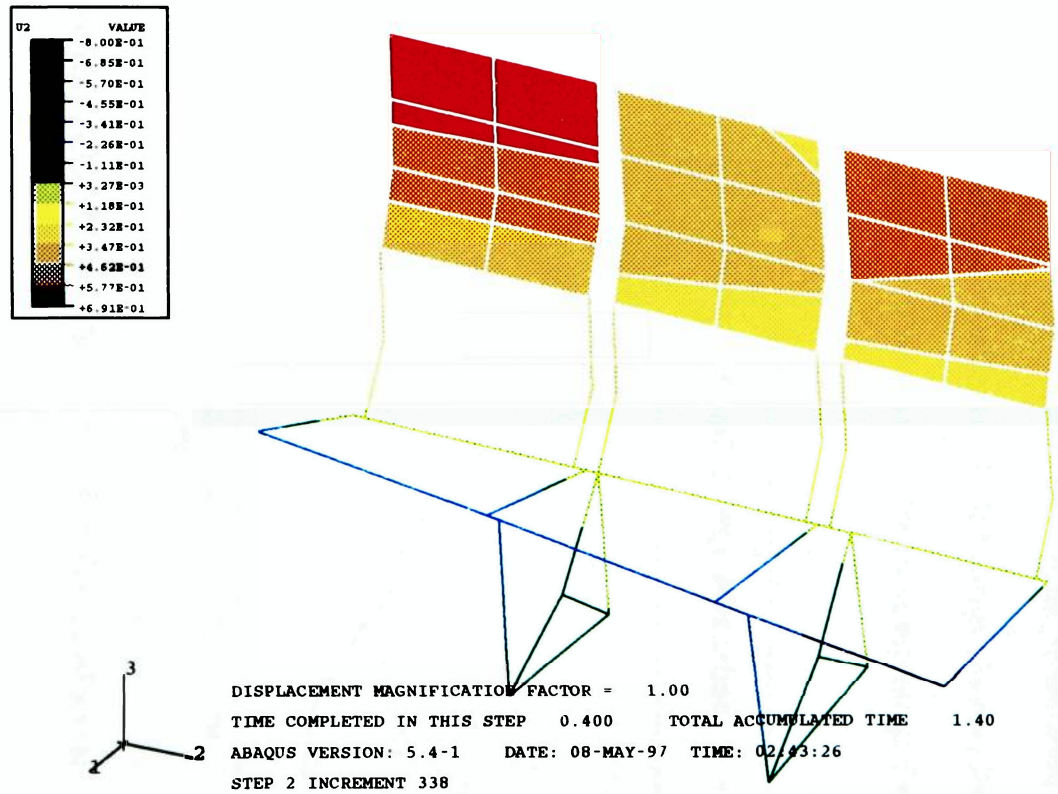


Figure 23. Lateral Deformation Contour of the seat

Figure 23 shows the final seat deformation of 0.8 in. in the lateral direction at the end of load application.

The energy absorbers constantly absorb energy throughout the test. It can be seen from figure 24 that the left energy absorber's axial stress remains constant at 41600 psi until 0.19 s. into the test. As the energy absorbers undergo plastic deformation, they allow the seat to deform in the forward direction, reducing the acceleration transmitted to the passenger. Load-deflection characteristics of the left energy absorber for this particular test is shown in figure 25. The area under the curve represents the total energy

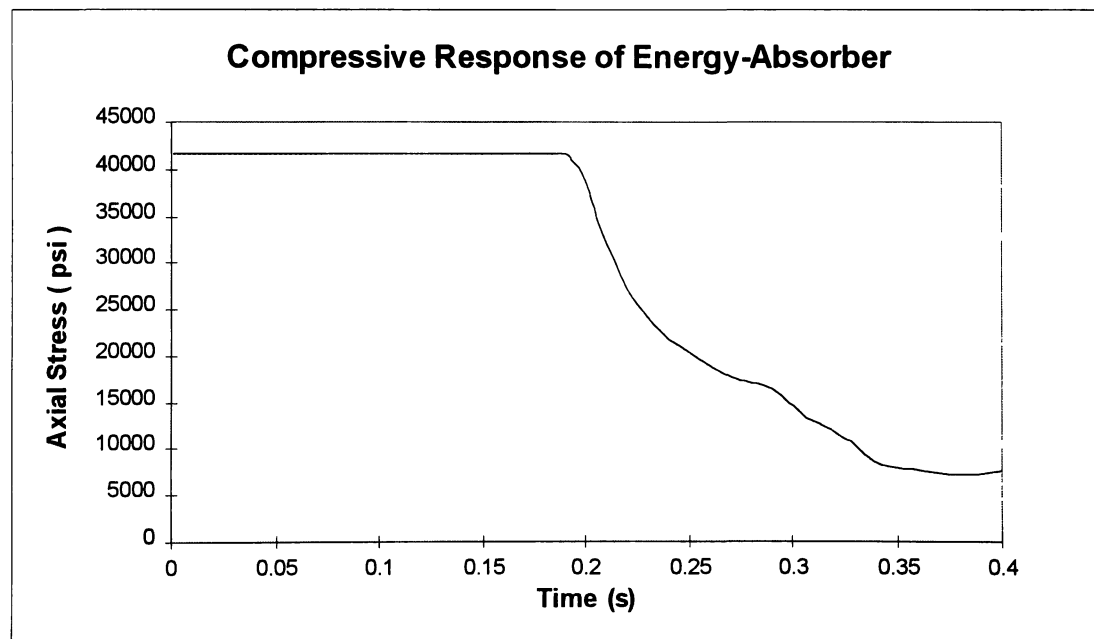


Figure 24. Time-History Compressive Stress of the Left Energy Absorber.

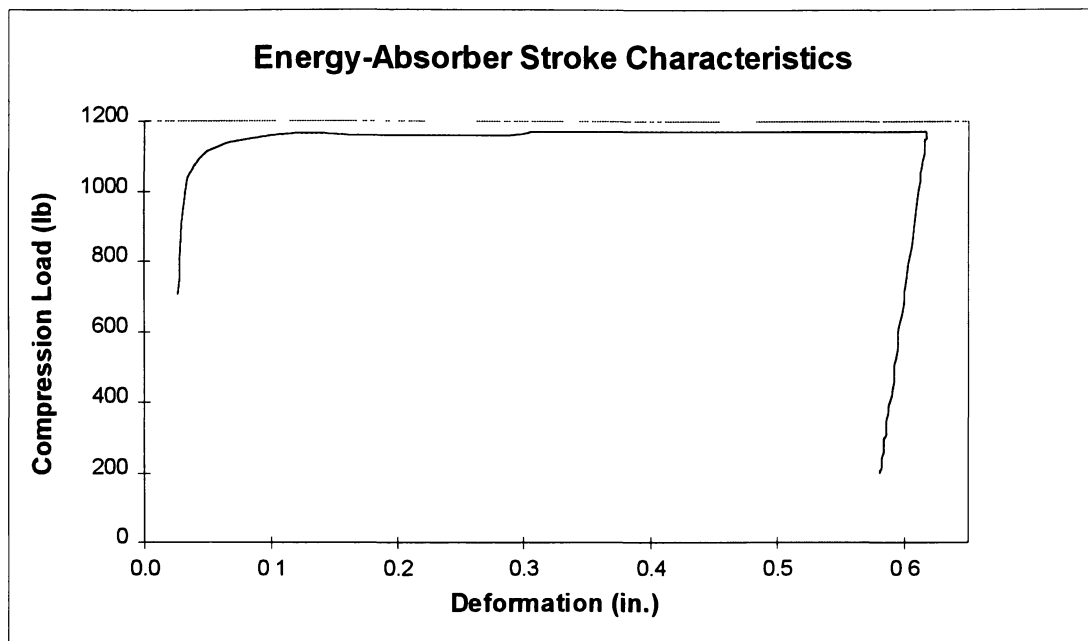


Figure 25. Force-Deflection curve of the Left Energy-Absorber for the 16g forward test

dissipated by this mechanism due to plastic deformation. It is approximately 720 lb-in. The total energy absorbed by the seat is 1,676 lb-in. The maximum deformation experienced by this mechanism is 0.6 in. The geometric characteristics of the legs do not allow greater axial deformation of these devices. Figure 26 shows a three dimensional view of the deformed seat.

The connection points of the rear and diagonal legs at the rear spar and the seat tracks are the structural locations that experience the highest levels of stresses. Members attached to these connection points experience very small amounts of plastic deformation. The highest Von-Mises stress that the structure experiences is only 4 % higher than the yielding stress.

ABAQUS

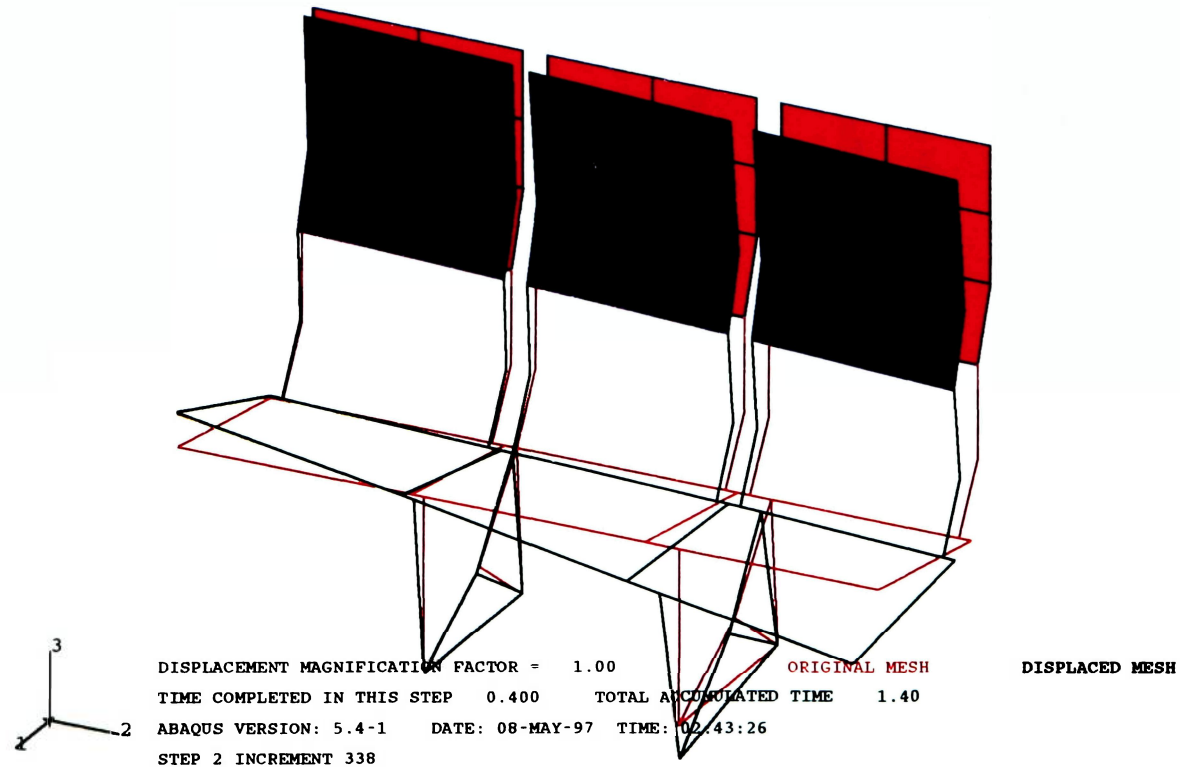


Figure 26. Three-Dimensional illustration of the deformed seat

When subjected to the 14g downward floor deceleration, the seat experiences very little forward deformation. The maximum forward deformation of 0.08 in. occurs at $t=0.108$ s. This translates to negligible amounts of energy absorption compared to those obtained in the previous test. Figure 27 shows a stress contour representation of the seat forward deformation at $t=0.108$ s. The seat is able to withstand the dynamic loading imposed in this test, but it provides no absorption of the crash energy. Figure 28 shows a contour of the Von-Mises stresses. The use of energy-absorption mechanisms that plastically deform at smaller loads could improve the performance of this seat. It would absorb more energy at the expense of more forward deformation. Too much deformation increases the chances of head injury due to impact with the seat in front.

There was no available information on the response of other energy-absorbing seats to compare the performance characteristics.

ABAQUS

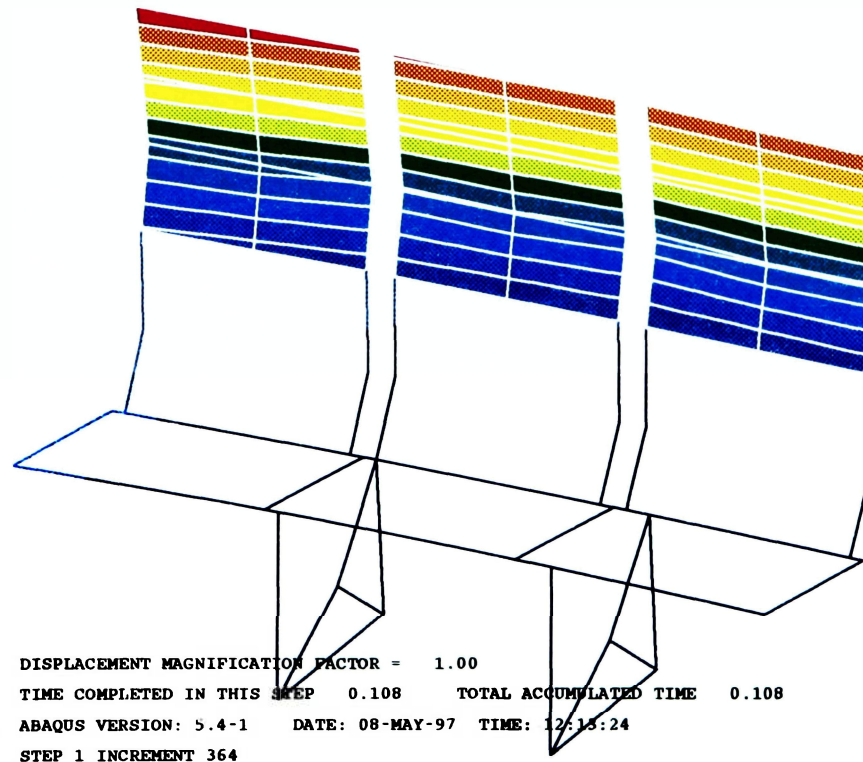
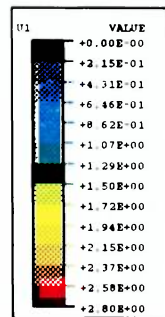


Figure 27. Forward deformation on the seat due to 14g floor deceleration

ABAQUS

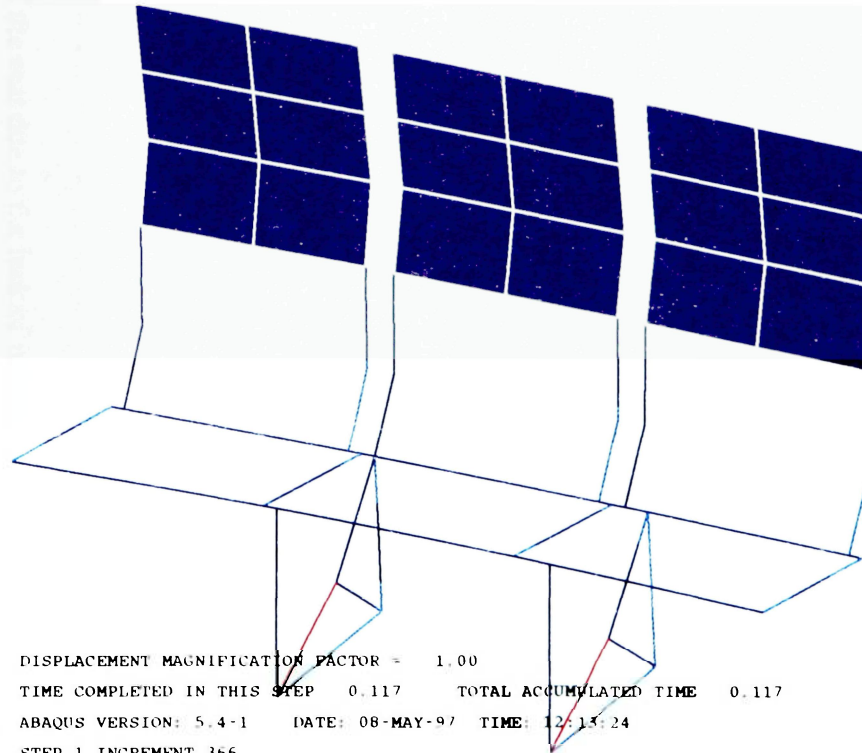
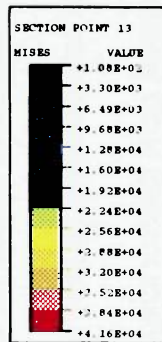


Figure 28. Von-Mises Failure criteria for 14g downward deceleration

5. CONCLUSIONS AND RECOMMENDATIONS

5.1. Conclusions

The passenger/seat interaction approach used to model the dynamic response analysis of the seat proved to be a good approximation of the load transfer scenario. While this approach did not accurately model the contact interference between the passenger and the seat, it provided a good enough mechanism of interaction to transmit the passenger inertia loads to the seat. Comparison between the results obtained from SOM-TA and ABAQUS showed that the predicted deformation of ABAQUS model closely followed the results obtained using SOM-TA.

The energy absorbing seat design is able to withstand the dynamic loading as stated in the emergency landing dynamic conditions section of the FAR part 25. The seat dissipated energy only when subjected to the 16g forward deceleration test. Plastic deformation of the energy absorbers was negligible in the 14g downward floor deceleration, since the leg assembly design of the seat does not provide the required degree of flexibility necessary to induce it. It was not possible to evaluate the performance of the seat due to the lack of information on other energy absorbing seats.

Nonlinear finite element analysis proved to be useful in the analysis of crashworthy passenger/seat systems. ABAQUS provides the necessary elements and modeling capabilities to analyze the mechanical behavior of structures under dynamic conditions. The ability to model nonlinear response is its greatest strength. ABAQUS

provides an automatic incrementation scheme in the solution process that makes it easy to use by inexperienced users.

Contact interference algorithms provided by ABAQUS were not able to model the interaction between the passenger and the seat. The algorithms did not converge to a solution for the contact problem.

ABAQUS can be used in a wide variety of applications. It has a large number of elements and material definitions as well as procedures library that makes it very versatile. It also gives the user the option to design new elements and materials. All of these features make ABAQUS a very powerful finite element program to be used for research. The unavailability of the pre-processor at Embry-Riddle greatly increased the time necessary to create models. The graphical interface provided by the post-processor made the analysis of the results significantly easier. It allows the animation of deformations of dynamic systems. It was used extensively to monitor the nonlinear response of the dummy.

5.2. Recommendations

A thorough analysis of the ABAQUS dummy response under a wide variety of dynamic conditions and accelerations is necessary to validate the model. Information on the dynamic response and failure modes of aircraft seats is not enough to obtain FAA certification. Loads at the pelvis and legs of the dummy as well as head acceleration curve are necessary to evaluate the injury criteria established by the regulations. Demonstration that this type of analytical method can accurately predict the seat mode of failure and the passenger response can allow the FAA to certify the seats as flightworthy. Comparison of the response of the seat model against data obtained from a test would give the FAA confidence in the response predicted using finite element analysis. This area is recommended for further investigation.

It is also recommended that a supercomputer be used to try to model passenger/seat contact effects using contact algorithms. The computer used for this research (Sun Sparc 1) is relatively slow. A computer with a greater degree of accuracy and higher processing speed may be able to provide the solution to the algorithm.

ABAQUS nonlinear capabilities can be used to design energy absorption mechanisms that can be used to control the loads and deformation of the seat for use in the general aviation and airline industry.

REFERENCES

1. Laananen, D.H., Simulation of Passenger Response in Transport Aircraft Accidents, Arizona State University, 1990.
2. National Transportation Safety Board, Cabin Safety in Large Transport Aircraft, September 9, 1981 (NTSB-AAS-81-2).
3. Code of Federal Regulations, Title 14-Civil Aviation, Part 25.562.
4. SAE International, Performance Standard for Seat in Civil Rotorcraft and Transport Airplanes, AS8049, 1990.
5. Desjardins, S.P., Cannon, M.R. and Shane, S.J., Discussion of Transport Passenger Seat Performance Characteristics, SAE Technical Paper Series, October 1989
6. Bolukbasi, A.O., and Laananen, D.H., Computer Simulation of a Transport Aircraft Seat and Occupant(s) in a Crash Environment, Volume I- Technical Report, Simula, Inc., August 1986 (DOT-FAA-CT-25-I).
7. Bolukbasi, A.O., and Laananen, D.H., Computer Simulation of a Transport Aircraft Seat and Occupant(s) in a Crash Environment, Volume II- Program SOM-TA User Manual, Simula, Inc., August 1986 (DOT-FAA-CT-25-II).
8. Ugural, A.C., Fenster, S.K., Advanced Strength and Applied Elasticity, PTR Prentice Hall, New Jersey, 1995.
9. Cook, R.D., D.S. Malkus and M.E. Plesha, Concepts and Applications of Finite Element Analysis, John Wiley & Sons, New York, 1989
10. Cook, R.D., Finite Element Modeling for Stress Analysis, John Wiley & Sons, 1995.
11. Kardestuncer, H., Finite Element Handbook, McGraw-Hill, 1987
12. Creager, M.W., An Investigation of the Floor Attachment Assembly of a Large Transport Aircraft Seat Subjected to Crash Dynamic Loadings, December 1991
13. Hibbitt, Karlsson & Sorensen, Inc, Abaqus/Standard, User's Manual, Volume I & II, 1994.
14. Backaitis, S.H., and Mertz, J.H., Hybrid III: The first Human-Like Crash Test Dummy, SAE International, 1994.

15. Kaleps, I., White, R.P., Measurement of Hybrid III Dummy Properties and Analytical Simulation Database Development, National Highway Traffic Safety Administration, February 1988.
16. Collins, J.A., Failure of Materials in Mechanical Design, John Wiley & Sons, New York, 1993.
17. Desjardins, S.P. and Laananen D.H., Aircraft Crash Survival Design Guide, Volume IV- Aircraft Seats, Restraints, Litters, and Padding, Simula, Inc., June 1980.